Spin rates of small moonlets embedded in planetary rings: I Three body calculations

Ryuji Morishima and Heikki Salo

Department of Physical Sciences, Division of Astronomy, P.O.BOX 3000 FIN-90014,

University of Oulu, Finland

Ryuji.Morishima@oulu.fi

Submitted to Icarus

Submitted June 3 2003

Revised August 27 2003

Manuscript pages: 49

Table: 0

Figures: 13

Proposed Running Head: Spin rates of moonlets in rings

Editorial correspondence to:

Ryuji Morishima

Department of Physical Sciences, Division of Astronomy, P.O.BOX 3000

FIN-90014, University of Oulu, Finland

Phone:+358-8-553-1944, Fax:+358-8-553-1934

e-mail: Ryuji.Morishima@oulu.fi

Abstract

We investigate the spin rates of moonlets embedded in planetary rings, subject to collisions with surrounding small particles, using three-body integrations including friction and spins. All successive impacts of the particle with the moonlet are followed, including a possible sliding phase after the initial inelastic rebounds. Two methods for treating impacts, 1) as instantaneous velocity changes and 2) using an impact force model, are applied after Salo (1995, *Icarus* 117, 287). Conducting a series of integrations with various initial summed spin velocity of the moonlet and the particle, we determine the equilibrium spin rate for which the averaged torque vanishes. This equilibrium spin rate corresponds to the final spin rate of the moonlet if the moonlet is much larger than the surrounding particles; it also corresponds to the mean spin rate for a ring composed of identical particles. We find that the equilibrium spin rate is enhanced by sliding orbits as compared with the spin rate determined by considering only the first impacts of the particles with the moonlet. If the random velocities of incident particles are small enough, the resulting equilibrium spin rate of the moonlet can be larger than the synchronous rotation rate, for $r_{\rm p}' \sim 1$, where $r_{\rm p}$ denotes the sum of radii of the colliding pair normalized by their mutual Hill radius. In this special case aggregates without internal strength may become rotationally unstable. However, the equilibrium spin rate decreases with increasing random velocity, and aggregates are always rotationally stable in the more likely case where the relative velocities are comparable to the mutual escape velocity. We also compare our results with the mean spin rates found in previous N-body simulations, and find a good agreement for optically thin rings; however the spin rates for optically thick rings are significantly larger than those predicted by our three-body calculations.

Key words: Planetary rings, Saturn

1 INTRODUCTION

Planetary rings, such as Saturn's rings, provide good local laboratories for studying the dynamics of flat collisional systems. In most parts of the rings, tidal force of the planet prevents ring particles from accreting into larger bodies. However, numerical N-body simulations suggest formation of apparently stable aggregates (moonlets) in outer parts of Saturn's A ring, if the internal density of particles is not much smaller than that of solid ice (Salo 1992, 1995, Karjalainen and Salo 2001). Existence of moonlets is suggested also in Saturn's F ring by Barbara and Esposito (2002), who showed that a moonlet collision model can consistently reproduce the localized brightenings seen in the Voyager images and during the ring plane crossing observations.

Unfortunately, observation of these hypothetical moonlets is quite difficult, because their expected size is under the resolution limit of Voyager cameras ($\sim$ 10 km), and because their total cross section is much smaller than that of the smaller particles. Using ground based stellar occultation observations, French and Nicholson (2000) estimated the upper limit for particle radius in the Saturn's A (and B) ring to be roughly 20m. However, a single power law distribution of particles sizes was assumed, which might not be applicable for moonlets made by runaway growth (see Barbara and Esposito 2002). Hence, the existence of moonlets with size of 100m–1km is still controversial.

If there are moonlets and the accretion of surrounding particles onto them continues, there would be no rings in these regions. Thus, there needs to be some mechanisms which break these moonlets, perhaps implying a balance between continuous accretion and breakup processes (e.g., Weidenschilling *et al.* 1984). Other possibility is that large moonlets clear gaps around them and thus avoid further accretion: the minimum size of a moonlet to be able to open a gap is estimated to be roughly 1 km (Spahn and Sremčević 2000, Daisaka *et al.* 2001, Sremčević *et*

al. 2002). Even in this case, one needs an explanation for why other particles do not continue to form other stable moonlets.

Besides its internal density, the spin rate of a moonlet is an important factor affecting its stability against the subsequent break up. Although there are many formulations related to the so-called classical Roche Limit, a model of Harris (1996) is quite simple to understand. He considered a solid, strengthless, spinning, and self-gravitating prolate ellipsoid and derived a simple expression for the distance $a_{\rm crit}$ inside which the disrupting centrifugal and tidal forces overcome the self-gravitating force (see also Davidsson 1999),

$$\frac{a_{\rm crit}}{R_*} = \left(\frac{2\rho_*/\rho}{1/f - (\omega/\omega_{\rm c})^2} \right)^{1/3}, \qquad (1)$$

where R_* and ρ_* are the radius and density of the planet, ρ is the density of the body, $f \geq 1$ is the axis ratio of the ellipsoid, ω is the spin frequency of the body, and $\omega_{\rm c}$ stands for the surface orbit frequency of the body ($\omega_{\rm c}{}^2 = 4\pi/3G\rho$). Eq. (1) suggests that an aggregate becomes more easily unstable ($a_{\rm crit}$ is larger) with an increased absolute value of the spin frequency.

Besides rotational instability, mutual collisions of moonlets offer a plausible mechanism for their breakup (Barbara and Esposito 2002). Also in this case, the pre-impact spin state is an important factor affecting the collision outcomes (Leinhardt *et al.* 2000).

Main factor to determine the spin rate of a moonlet, whether it is a strengthless aggregate or a cohesive body having a non-zero yield strength, is likely to be the collisions and/or accretion of surrounding particles. Also for the moonlets in gaps, like Pan in the Encke gap (Showalter 1991), their rotation is likely to be determined by accretion processes of small particles, since the time scale to reach synchronous tidal locking is very long for such small bodies. If more moonlets will be found, whether these reside in gaps or not, and their spin states can be clarified (though it is questionable if this is possible even by the Cassini mission), this will help to constrain many physical parameters for the moonlets and small ring particles, such as the internal

densities and the coefficient of restitution, by comparing with theoretically expected values.

There are many studies about the collisional evolution of spins of celestial bodies. A lot of studies have addressed the problem of how planetary spins are determined by planetesimal accretion, usually assuming a perfect accretion (e.g., Ida 1990, Lissauer and Kary 1991, Dones and Tremaine 1993, Ohtsuki and Ida 1998). In the case of planetary rings, however, the accretion probability of colliding particles becomes small due to the planetary tide (Ohtsuki 1993). In this case, the spin rate of a moonlet is determined by inelastic rebounds of small particles, including multiple hits of the same particle, possibly occurring with very small time intervals (so-called "sliding phase": see Petit and Hénon 1987, Wisdom and Tremaine 1988).

Salo (1987b) performed numerical simulations of the collisional evolution of ring particles, including spins of particles (and thus also frictional force). He obtained ratios of the kinetic energy of spin motions to that of the random motions, as well as determined the dispersion and the mean spin of the particles, but only in the case where self-gravity of particles was neglected. Also some theoretical calculations exist for the spin evolution of ring particles (Salo 1987a, Araki 1991, Hämeen-Anttila and Salo 1993). According to these studies, the particles' mean spin acquires a nonzero vertical component, of about 0.3 times the orbital frequency, depending only little on various parameters (optical depth, elasticity model), consistent with numerical results in Salo (1987b). However, in these theoretical studies, self-gravity of particles was included only approximately (the mean vertical gravitational field and the scattering by binary encounters), so that the effects of accretion and multiple impacts were not included.

In subsequent local N-body simulations with self-gravitating particles by Salo (1995), some runs included friction and spins of particles, and it was found that the vertical component of the mean spin is much larger than the above theoretical expectation. Examples of aggregate formation were also given in Salo (1995), but the longterm stability or spin evolution of aggre-

gates was not studied in detail. The used local method, with periodic boundary conditions, is not well suited for this purpose. Namely, if the conditions for aggregate formation are satisfied, then most of the mass becomes rapidly contained in one or few aggregates, and there are little further collisions by small particles, in comparison to a realistic ring where a continuous flow of particles is supplied by the surrounding regions. Also, to study the subsequent evolution of the aggregate in a realistic manner, the supply of new particles would need to correspond to a non-perturbed ring region, violating the strict periodicity assumed in the code. Thus, the existing local simulations (Salo 1992, 1995; Karjalainen and Salo 2003, in preparation) have limitations in their relevance to the evolution of spin rates of the aggregates.

On the other hand, three body calculations provide an easier way to investigate the effects of collisions and self-gravity of particles, at least in the low optical depth limit. In this case, the flow of particles is a given Keplerian flow, and each particle-moonlet interaction is treated separately from all others. Using numerical calculations of three body problem, Petit and Hénon (1987) examined the sliding phase and the evolution of the velocity dispersion of particles by inelastic collisions and gravitational encounters. However, they did not include friction nor spins of the particles. Ohtsuki (1993) examined the capture probability of colliding particles with various normal and tangential restitution coefficients. He did not consider spins of particles, in other words, the particles were assumed to keep the synchronous rotation, with no exchange of energy between random motions and spin motions. Thus, the evolution of spins was not clarified.

In the present paper, conducting three body orbital integrations including spins and friction, we examine the collisional evolution of spin rates of moonlets embedded in a swarm of smaller particles. Actually, the method to obtain the final spin rates of moonlets is completely the same as that to obtain the mean spin rate for a ring of identical particles, so that we can compare our

results with those obtained by previous N-body simulations. We also calculate the capture probability of colliding particles, in a similar fashion as Ohtsuki (1993). Further, we also calculate the sliding probability representing the rate of temporally (but not permanently) captured orbits. Throughout our calculations, we compare the two different methods for treating collisions used in Salo (1995).

Ohtsuki (2003a, b) also address the same topic of this paper, and his and our studies are complementary to each other. Taking into account the Rayleigh distribution of orbital eccentricities and inclinations of impacting particles, he estimated not only the systematic (averaged) component but also the random component of the moonlet spin, which arises from the collisions of large impactors; this is not considered in the present paper studying just the systematic component. The reader is recommended to read these papers as well.

In the present study, we assume that the moonlet and colliding particles are spherical and do not have surface irregularity, and that there is no sticking force between contacting bodies. As a result, the sliding phase plays a significant role in determining the final spin of a moonlet. Hence, we make a special effort to investigate the sliding phase as accurately as possible. It should be noted, however, that the assumption of spherical particles without surface irregularity is a highly idealized model. Hence, one should be careful when applying the results in the present paper to realistic rings. Nevertheless, it is clear that one needs first to understand the ideal case before continuing to the more realistic (and thus more complex) case.

In Section 2, we describe our methods for calculating collisions. In Section 3, we describe the basic orbital behavior of particles in the sliding phase. In Section 4, we show the dependence of the moonlet spin on various parameters, like the strength of gravity and friction. In Section 5, we compare our results with those of Ohtsuki(2003a ,b), discuss briefly the stability of rubble pile aggregates, and moreover compare our results with those obtained in earlier

N-body simulations. Finally, our conclusions are given in Section 6.

2 METHODS

2.1 Hill's Equations

Consider a moonlet experiencing collisions with surrounding ring particles and orbiting around a planet. We examine the spin rate of the moonlet determined by the collisions of ring particles, subject to the tidal field and the moonlet's gravity. To describe the motion of these bodies, we adopt the Hill's approximation which assumes that the masses of the ring particles and the moonlet are much smaller than the planet's mass and that their random velocities are much smaller than the Keplerian velocity around the planet. We adopt a rotating local Cartesian coordinate with the origin at the center of the moonlet, with the x-axis pointing radially outward from the planet, the y-axis pointing in the orbital direction, and the z-axis pointing in the direction perpendicular to the orbital plane according to the right-hand rule. The equations describing the relative motion between a ring particle and the moonlet are given by Hill's equation (e.g., Petit and Hénon 1986, Nakazawa and Ida 1988):

$$\begin{aligned} \ddot{x} &= +2\dot{y} + 3x - \frac{3x}{r^3} \\ \ddot{y} &= -2\dot{x} - \frac{3y}{r^3} \\ \ddot{z} &= -z - \frac{3z}{r^3}, \end{aligned} \tag{2}$$

where $r = (x^2 + y^2 + z^2)^{1/2}$. The above equations are written in a non-dimensional form: time is normalized by the inverse of the Keplerian angular velocity of the moonlet Ω^{-1}, and length is normalized by the Hill radius given by

$$R_{\rm H} = ah = a\left(\frac{m_1 + m_2}{3M_*}\right)^{1/3}, \tag{3}$$

where a is the semimajor axis of the moonlet, h is the reduced Hill radius, M_*, m_1, and m_2 are the masses of the planet, the moonlet, and the ring particle, respectively. In the following, we use normalized quantities unless otherwise indicated.

[Figure 1]

The relative strength of the gravity to the tidal force of the planet is characterized by r_p parameter, defined as the sum of the radii of the moonlet and the particle, normalized by the Hill radius. For Saturn's rings,

$$r_\mathrm{p} = r_1 + r_2 = 0.77 \left(\frac{D\rho}{900 \text{ kg m}^{-3}} \right)^{-1/3} \left(\frac{a}{10^8 \text{ m}} \right)^{-1} \frac{1 + (D\mu)^{1/3}}{(1+\mu)^{1/3}}, \tag{4}$$

where r_1 and r_2 are the physical radii of the moonlet and the small particle normalized by R_H, ρ is the internal density of the small particles, $\mu = m_2/m_1$, and D denotes the volume filling factor of the moonlet. The value $\rho = 900$ kg m^{-3} corresponds to the density of non-porous solid ice, while the density of the aggregate, $D\rho$, may be smaller due to voids. Figure 1 illustrates the dependence of r_p on a for Saturn's rings, for various values of ρ, D, and μ. We conduct our calculations for a wide range of non-dimensional radii, $0.5 \le r_\mathrm{p} \le 2.0$, covering well the tidal environment in planetary rings.

When the ring particle is far from the moonlet and thus their mutual gravity is negligible, the solution of Eq. (2) is given by the epicyclic motion,

$$\begin{aligned} x &= b - e\cos(t-\tau) \\ y &= -\frac{3}{2} b(t-\phi) + 2e\sin(t-\tau) \\ z &= i\sin(t-\lambda), \end{aligned} \tag{5}$$

where ϕ defines the origin of time (we choose $\phi = 0$ and thus the possible impacts occur near $t = 0$), $b = (a_2 - a)/R_\mathrm{H}$ stands for the impact parameter, i.e., difference in the initial semimajor

axis (where a_2 is the semimajor axis of the small particle), $e = e^*/h$, $i = i^*/h$ for the reduced eccentricity and the reduced inclination (where e^* and i^* are the eccentricity and the inclination in the ordinary use), τ, and λ for the longitude of pericenter, and the longitude of ascending node, respectively (see Nakazawa and Ida 1988 for details). We set the initial azimuthal distance as $|y_0| = \max(40, 20e)$ which is large enough for neglecting the mutual gravity. We mainly show the results for the case of $e = i = 0$, but also discuss the cases with different values of e (≤ 3.5), with fixed $e/i = 2$. This range of e covers well the plausible range of velocity dispersion $v_r = \sqrt{e^2 + i^2}$, since the escape velocity of the moonlet equals $v_{\rm esc} = \sqrt{6/r_{\rm p}}$; the e/i ratio approximates that found in low optical depth rings dominated by gravitational encounters (Ida 1990, Ohtsuki 1999).

We numerically integrate Eq. (2) using a fourth-order variable time-step Runge-Kutta method and calculate the torque exerted on the moonlet by the collisions of particles. When the particle is far enough from the moonlet, the typical time step is $\sim 10^{-2}$, whereas it is shortened to $\sim 10^{-4}$ near the moonlet in order not to miss any collisions. Details of treating the collisions are explained in next subsection. Each orbital integration is continued until the particle goes far away from the moonlet ($|y| > |y_0|$ with $t > 0$), or until the Jacobi energy E becomes negative, as adopted in Ohtsuki (1993), where E is the energy integral of Eq. (2) given by

$$E = \frac{1}{2}(\dot{x}^2 + \dot{y}^2 + \dot{z}^2) - \frac{3}{2}x^2 + \frac{1}{2}z^2 - \frac{3}{r} + \frac{9}{2}. \tag{6}$$

Small particles colliding with the moonlet have initially positive values of E, but if E becomes negative after some collisions the particle can not escape from the moonlet. Strictly speaking, negative E does not always guarantee the capture, since we include the spins of small particles and the additional pressure force at the time of impact. However, we find that an escape of a particle after its Jacobi energy becomes negative is very rare, and therefore use the condition $E < 0$ for the capture. It is clear that the capture is not possible if $r_{\rm p} > 1$, in which case all the

points on the surface of the moonlet extend beyond the Hill's surface ($E > 0$ even for a zero relative velocity).

In order to obtain accurate results, we need to divide the orbital parameter space into a fine grid. In the case of $e = i = 0$, we sample the impact parameter with $\Delta b = 0.003$. In the case of $e \neq 0$, we adopt $\Delta b = 0.1$ and use divisions of τ and λ as $(2\pi/\Delta\tau, \pi/\Delta\lambda) = (40, 20)$. Using these divisions of parameters, we find about a few hundreds and five thousands colliding orbits in each parameter set for $e = i = 0$ and $e \neq 0$, respectively. Additional tests with a finner grid indicate that our results are not significantly changed.

2.2 Treatment of Impacts

Two different methods are used in the calculations of impacts, following Salo (1995): in the first method, the locations of impact points are searched and the corresponding instantaneous velocity changes are calculated, whereas, in the second method, particle orbits are integrated through impacts, including additional visco-elastic forces arising between the slightly overlapping particle and moonlet. The latter method has significant advantages for N-body simulations of dense self-gravitating systems (e.g., Salo 1995, Salo *et al.* 2001), although it uses more CPU time relative to the first method in three body calculations. We briefly describe both methods in the following.

In terms of the relative velocity $\boldsymbol{v} = (\dot{x}, \dot{y}, \dot{z})$, the velocity difference $\boldsymbol{u}$ at the contact point is given by

$$\boldsymbol{u} = \boldsymbol{v} - r_{\rm p}(\boldsymbol{\omega}_{\rm p} - \boldsymbol{N}) \times \boldsymbol{n}, \tag{7}$$

with

$$\boldsymbol{\omega}_{\rm p} = \frac{r_1\boldsymbol{\omega}_1 + r_2\boldsymbol{\omega}_2}{r_{\rm p}}, \tag{8}$$

where $\boldsymbol{n}$ is the unit vector pointing to the direction of the center of the small particle, $\boldsymbol{\omega}_1$, $\boldsymbol{\omega}_2$, $\boldsymbol{\omega}_\mathrm{p}$ are the spin angular velocity vector of the moonlet, that of the small particle, and the averaged spin vector in the inertial (not rotating) co-ordinate system, respectively, and $\boldsymbol{N}$ is the unit vector in the z direction. Note that in Eq. (7), $\boldsymbol{\omega}_\mathrm{p} - \boldsymbol{N}$ represents the spin vector in the rotating co-ordinate system and that the components of the inertial spin vector $\boldsymbol{\omega}_\mathrm{p}$ need to be expressed with respect to the instantaneous axis directions of the rotating system. Therefore, the equatorial components of $\boldsymbol{\omega}_\mathrm{p}$ change even between collisions as

$$\frac{d\boldsymbol{\omega}_\mathrm{p}}{dt} = \boldsymbol{\omega}_\mathrm{p} \times \boldsymbol{N}. \tag{9}$$

(1) *Instantaneous impact model*

In the first method, the post-collisional velocity difference $\boldsymbol{u}'$ is given by (Salo 1987a, Richardson 1994)

$$\boldsymbol{u}' = -\varepsilon_\mathrm{n}\boldsymbol{u}_\mathrm{n} + \varepsilon_\mathrm{t}\boldsymbol{u}_\mathrm{t}, \tag{10}$$

where ε_n and ε_t stand for the normal and tangential restitution coefficients ($\varepsilon_\mathrm{t} = 1$ corresponds to a frictionless impact: note that our ε_t was denoted by $(1 - \beta)$ in Salo 1987a and by $(1 - \varepsilon_\mathrm{t})$ in Salo 1995, respectively), and $\boldsymbol{u}_\mathrm{n} = (\boldsymbol{u} \cdot \boldsymbol{n})\boldsymbol{n}$ and $\boldsymbol{u}_\mathrm{t} = \boldsymbol{u} - \boldsymbol{u}_\mathrm{n}$ are the normal and tangential components of the pre-collisional velocity difference at the contact point, respectively.

The changes of the relative velocity and the spin vectors are derived from the conservation of linear and angular momentum as

$$\boldsymbol{v}' - \boldsymbol{v} = -(1 + \varepsilon_\mathrm{n})\boldsymbol{u}_\mathrm{n} - \frac{\alpha}{1 + \alpha}(1 - \varepsilon_\mathrm{t})\boldsymbol{u}_\mathrm{t}, \tag{11}$$

$$r_\mathrm{p}\boldsymbol{\omega}_\mathrm{p}' - r_\mathrm{p}\boldsymbol{\omega}_\mathrm{p} = \frac{1}{1 + \alpha}(1 - \varepsilon_\mathrm{t})\boldsymbol{n} \times \boldsymbol{u}_\mathrm{t}, \tag{12}$$

where $\boldsymbol{v}'$ and $\boldsymbol{\omega}_\mathrm{p}'$ are the relative velocity and the averaged spin vector after the impact, respectively, and α is the effective moment of inertia of the colliding pair, whose moments of inertia

are $J_1 = \alpha_1 m_1 {R_1}^2$ and $J_2 = \alpha_2 m_2 {R_2}^2$, defined by

$$\frac{1}{\alpha} = \frac{m_1 m_2}{m_1 + m_2}\left(\frac{1}{m_1\alpha_1} + \frac{1}{m_2\alpha_2}\right). \tag{13}$$

In what follows, we assume that both the particle and the moonlet have a homogeneous internal mass distribution, so that $\alpha_1 = \alpha_2 = \alpha = 2/5$. Changes in the spin velocity of the moonlet $r_1\omega_1$ and in the spin velocity of the small particle $r_2\omega_2$ are obtained by multiplying Eq. (12) with $\mu/(1+\mu)$ and $1/(1+\mu)$, respectively. Thus, the collision outcome for an arbitrary mass ratio μ can be obtained by one orbital calculation.

If we find overlapping of the small particle and the moonlet during the integration, we go back one step, to the time before the impact, and analytically estimate the location and velocity of the impact using a second-order Taylor expansion for the particles' mutual separation. Then changing the velocity and the spin vectors following Eqs. (11) and (12), we extrapolate the position and velocity to the end of this time step, and continue the integration with the Runge-Kutta method. If we simply change the velocity after finding an overlap, without using the above way for correcting to the more accurate impact time, this easily leads to an error that the particle sinks deeper into the moonlet.

In the sliding phase, we set $\varepsilon_{\rm n}$ to unity if the perpendicular component of impact velocity is smaller than $u_{\rm n,crit} = 0.01$, as adopted in previous studies (Wisdom and Tremaine 1988, Ohtsuki 1993, Salo 1995). We find that we can not exclude errors caused by sinking of the small particle into the moonlet without this treatment. Note, however, that the efficiency of friction depends on $u_{\rm n,crit}$ (see Appendix A).

(2) *Force model*

In this method, the normal force exerted between the overlapping particle and the moonlet is given by the linear visco-elastic model of Dilley (1993), and the tangential force is also included.

The additional translational acceleration $\dot{\boldsymbol{v}}_{\rm add}$ arising between the overlapping, colliding pair is modeled as

$$\dot{\boldsymbol{v}}_{\rm add} = -\ddot{\xi}(\boldsymbol{n} - \frac{\alpha}{1+\alpha}\ell_{\rm f}\boldsymbol{n}_{\rm t}), \tag{14}$$

with

$$\ddot{\xi} = \begin{cases} -\omega_0^2\xi - \dfrac{\dot{\xi}}{s}, & (\xi \geq 0), \\ 0 & (\xi < 0), \end{cases} \tag{15}$$

where $\xi = r_{\rm p} - |\boldsymbol{r}|$ is the penetration depth, $\ell_{\rm f}$ denotes the coefficient of friction, and $\boldsymbol{n}_{\rm t} = \boldsymbol{u}_{\rm t}/|\boldsymbol{u}_{\rm t}|$ is the unit vector pointing in the tangential direction. In the above, ω_0 is the undamped frequency of the harmonic impact force, and s is the characteristic time of damping, respectively. The equation for averaged spin motion is given by

$$\frac{d(r_{\rm p}\omega_{\rm p})}{dt} = -\frac{1}{1+\alpha}\ell_{\rm f}\ddot{\xi}\boldsymbol{n} \times \boldsymbol{n}_{\rm t}, \tag{16}$$

where α is the factor defined in Eq. (13). Note that the spin evolution of the moonlet and the small particle can be obtained by multiplying with the same mass coefficients as in the case of Eq. (12).

The attractive characteristic of the linear force model is that the parameters ω_0 and s can be tied to the normal restitution coefficient $\varepsilon_{\rm n}$, and the duration of the impact (Salo 1995). The solution of Eq. (15) for $\xi \geq 0$ is given by

$$\xi = \frac{\dot{\xi}(0)}{\omega_{\rm m}} e^{-t/2s} \sin(\omega_{\rm m} t), \tag{17}$$

where $\omega_{\rm m}$ is the modified frequency given by

$$\omega_{\rm m} = \sqrt{\omega_0^2 - 1/(2s)^2}. \tag{18}$$

Using the above equations, the normal restitution coefficient is described as

$$\varepsilon_{\rm n} = -\frac{\dot{\xi}(\pi/\omega_{\rm m})}{\dot{\xi}(0)} = e^{-\pi/2\omega_{\rm m} s}, \tag{19}$$

where the impact starts $t = 0$ and finishes $t = \pi/\omega_{\rm m}$. We adopt $\omega_0 = 200$, which is the same value as used in Salo (1995). In fact, the impact duration ($\sim T_{\rm K}/(2\omega_0)$ where $T_{\rm K}(= 2\pi)$ is the orbital period) derived from this value of the frequency is much longer than realistic collision time (< 1 sec, in the dimensional form), but we checked that results do not differ from those obtained by using a higher value of ω_0. This scaling of the impact duration to be longer than the physical impact duration is very convenient as it allows the use of larger integration steps. After ω_0 is fixed, the damping parameter s is determined by the desired $\varepsilon_{\rm n}$ via Eqs. (18) and (19).

If we include the gravity term $3/r_{\rm p}^2$ from Eq. (2) into Eq. (15), a constant term $3/(r_{\rm p}\omega_0)^2$ is added to the solution Eq. (17). Note that this term is generally negligible for the first hit of each particle. However, when the normal component of the impact velocity is reduced by several impacts, the gravity term can become significant, and Eq. (19) becomes a wrong description for $\varepsilon_{\rm n}$ since the solution of ξ remains slightly positive, which means the sliding phase. This is the one of fundamental differences from the instantaneous method, in which the sliding phase is always described by a sequence of small impacts. However, as in this case no energy is lost via inelasticity, this corresponds to setting $\varepsilon_{\rm n} = 1$ in the instantaneous impact method when $u_{\rm n} < u_{\rm n,crit}$.

The other important difference is the way of describing friction. Comparing the normal and tangential components of velocity change in each impact for both impact models, the relation between the friction coefficient $\ell_{\rm f}$ and the tangential restitution coefficient $\varepsilon_{\rm t}$ is given by

$$\ell_{\rm f} = \frac{(1-\varepsilon_{\rm t})}{(1+\varepsilon_{\rm n})}\frac{|\boldsymbol{u}_{\rm t}|}{|\boldsymbol{u}_{\rm n}|}. \tag{20}$$

Thus, if $\varepsilon_{\rm t}$ is constant $\ell_{\rm f}$ can not be a constant and vice versa, and either one should have an impact-angle dependence. The laboratory experiments of ice particle collisions by Supulver *et al.* (1995) showed that the value of $\varepsilon_{\rm t}$ is about 0.9 for glancing 1cm sec^{-1} impacts, also

suggesting that ε_t becomes smaller for more perpendicular impacts. This seems to be consistent with ℓ_f rather than ε_t being constant. Unfortunately, since they did not clearly show the impact-angle dependence of ice particle collisions (they only showed that for rubber ball collisions), we do not know how accurately ℓ_f is constant; there is also a possibility that neither ℓ_f nor ε_t is independent of impact angle. In any case, experiments by Supulver *et al.* (1995) suggest that the value of ℓ_f is small (< 0.1).

Taking into account the above uncertainties we think that it is worth compare both methods, with a range of different friction parameters, and study the differences in the implied spin states in the rings. It should also be noted that for the initial impact in each encounter, the average value of $|\boldsymbol{u}_t|/|\boldsymbol{u}_n|$ is expected to be about unity, whereas in the sliding phase this value becomes much larger than unity. Therefore, if ε_t is constant, the strength of friction ($\propto (1-\varepsilon_t)$) in the sliding phase is strongly overestimated compared with the case of ℓ_f being fixed.

In numerical integrations using the force model, we find that a large relative error occurs in $\boldsymbol{u}_t$ when $|\boldsymbol{u}_t| \sim 0$, in which case the numerical time step is automatically shortened too much. This follows from the discontinuity of tangential force at $|\boldsymbol{u}_t| \sim 0$. In order to avoid this discontinuity, we replace $\boldsymbol{n}_t = \boldsymbol{u}_t/|\boldsymbol{u}_t|$ by $\boldsymbol{u}_t/u_{t,crit}$ if $|\boldsymbol{u}_t| < u_{t,crit} = 0.001$. However, the results are not sensitive to the exact choice of $u_{t,crit}$.

2.3 Method for Obtaining the Equilibrium Spin Rate

Using the two types of impact methods described above, we calculate the torque exerted on the moonlet by the collisions of small particles. This is obtained by evaluating the spin change $\Delta\boldsymbol{\omega}_p$ in each orbital integration and averaging it over all impacting orbits. In the case that the particle escapes from the moonlet, this change is obtained simply from the difference between the final and initial $\boldsymbol{\omega}_p$. However, if the small particle is captured, we put the final spin

velocity as $\boldsymbol{\omega}_{\rm p} = \boldsymbol{N}$, instead of using the instantaneous value at the time when the numerical integration is terminated. This treatment is justified, as N-body experiments indicate that the captured particles eventually accumulate at the the subplanet points $(x, y, z) = (\pm r_{\rm p}, 0, 0)$, with $\boldsymbol{u} = \boldsymbol{v} = 0$, which according to Eq. (7) implies $\boldsymbol{\omega}_{\rm p} = \boldsymbol{N}$.

Conducting the calculations with various initial spin rates $\boldsymbol{\omega}_{\rm p,ini}$, we determine the equilibrium spin rate $\boldsymbol{\omega}_{\rm p,eq}$ for which the averaged torque vanishes ($\langle \Delta\boldsymbol{\omega}_{\rm p} \rangle = 0$). It should be noted that the equatorial components of the averaged torque must vanish when $\omega_{{\rm p,ini},x} = \omega_{{\rm p,ini},y} = 0$, because of the symmetry of the distribution of impacting particles with respect to z and $\dot{z}$, so that we only need to consider the z-component of the averaged torque. In the following, we omit the subscript z from the z components of spins, in order to avoid complicated expressions (e.g., $\omega_{\rm p,eq} \equiv \omega_{{\rm p,eq},z}$).

In the equilibrium state, the following equation is satisfied,

$$r_{\rm p}\omega_{\rm p,eq} = r_1\langle\omega_1\rangle + r_2\langle\omega_2\rangle \tag{21}$$

where $\langle\omega_1\rangle$ and $\langle\omega_2\rangle$ represent the averaged spin angular velocities of the moonlets and the incoming particles (consider averaging over a lot of moonlets independently surrounded by small particles, or equivalently, time averaging about one moonlet). If there are enough mutual collisions between small particles, $\langle\omega_2\rangle$ is expected to be less than unity (e.g., Salo 1987b), and as we show later $\omega_{\rm p,eq}$ is also of order of unity. Thus, if we consider the case $r_1 \gg r_2$, the second term in the right hand side of Eq. (21) is negligible, so that we can treat $\omega_{\rm p,eq}$ itself as the equilibrium (or time averaged) spin rate of the moonlet $\langle\omega_1\rangle$. On the other hand, if we consider collisions of identical particles ($r_1 = r_2$ and $\langle\omega_1\rangle = \langle\omega_2\rangle$), one can immediately find that $\omega_{\rm p,eq}$ represents $\langle\omega_1\rangle$ also in this case. Thus, we can also check our 3-body results by comparing with N-body simulations of identical particles.

3 SLIDING PHASE

[Figure 2]

Before studying the dependence of the equilibrium spin rate on various parameters like the strength of gravity and friction, we describe the typical orbital and spin evolution, focusing on the sliding phase. Figure 2 shows (a) an example of colliding orbit including the sliding phase and (b) the corresponding evolution of physical quantities as functions of time, obtained by the instantaneous impact model. After some large rebounds, the particle in Fig. 2 starts to slide on the moonlet in the retrograde direction ($\dot{\theta} < 0$, where we adopt cylindrical co-ordinates (r, θ); $(x, y) = (r\cos\theta, r\sin\theta)$), as seen in the rotating frame. During the sliding phase, the relative tangential velocity at the contact point, $u_\theta = r\dot{\theta} - r_{\rm p}(\omega_{\rm p} - 1)$, remains small because the spin rate more or less compensates the rotation rate ($\omega_{\rm p} - 1 \simeq \dot{\theta}$). This happens unless the friction strength $1 - \varepsilon_{\rm t}$ (or $\ell_{\rm f}$ for the force model) is too small. The Jacobi integral E oscillates due to the exchange between the spin energy and the translational kinetic energy, but on the average E decreases with time due to frictional energy loss. With decreasing E, the time averaged value of $\dot{\theta}$ increases. Finally, the sliding direction around the moonlet switches to the prograde direction ($\dot{\theta} > 0$), after that the particle escapes from the moonlet almost immediately. It should be noted that the spin experiences a large jump shortly before escape. Qualitatively same results are obtained also when using the force model, or with different strengths of friction.

3.1 Analytic Solution for Sliding Motion

The basic behavior in Fig. 2 can be easily understood by the analytical solution of the sliding phase, derived by Petit and Hénon (1987). Introducing cylindrical co-ordinates and neglecting

friction, the equation of motion in the two-dimensional case is written as

$$\begin{aligned} \ddot{r} &= r\dot{\theta}^2 + 2r\dot{\theta} + 3r\cos^2\theta - \frac{3}{r^2} + \gamma \\ \ddot{\theta} &= -\frac{2\dot{r}}{r}(\dot{\theta} + 1) - \frac{3}{2}\sin 2\theta, \end{aligned} \tag{22}$$

where γ denotes the radial acceleration due to the pressure force between contacting particles. In the sliding phase, $r \approx r_\mathrm{p}$, and thus $\dot{r} = \ddot{r} = 0$. Therefore we need only study the behavior of θ with time. Multiplying Eq. (22) by $\dot{\theta}$ and integrating, we obtain

$$\dot{\theta} = \pm\sqrt{3\cos^2\theta + C}, \tag{23}$$

where the constant of integration C is related to the Jacobi integral as $C = 2(E + 3/r_\mathrm{p} - 9/2)/r_\mathrm{p}^2$. If C is positive, the solution corresponds to a retrograde ($\dot{\theta} < 0$) or prograde ($\dot{\theta} > 0$) revolution around the moonlet. If C is negative (but $C > -3$), it describes an oscillation around $\theta = 0$ or π, $\dot{\theta}$ obtaining both negative and positive values. In Fig. 2, C is positive at first, which corresponds to $E > 0.75$, and the particle revolves around the moonlet in a retrograde direction. After C becomes negative, the type of motion is changed. If the gravity is sufficiently strong so that the particle can keep its sliding motion, it starts to oscillate on the moonlet. But in the case of Fig. 2, the particle escapes practically immediately after C becomes negative.

This escape can be understood by estimating the radial acceleration. Substituting Eq. (23) into Eq. (22), the condition for maintaining the sliding phase ($\ddot{r} < 0$ for $\gamma = 0$) is written as

$$6\cos^2\theta + C \pm 2\sqrt{3\cos^2\theta + C} < \frac{3}{r_\mathrm{p}^3}. \tag{24}$$

The left hand side attains its maximum when $\theta = 0$ or π. Thus, putting $C = 0$, the condition for keeping retrograde rotation around the moonlet becomes

$$r_\mathrm{p} < r_{\mathrm{p},1} = \left(\frac{3}{6 - 2\sqrt{3}}\right)^{1/3} = 1.058. \tag{25}$$

On the other hand, the condition for maintaining the sliding phase after the type of motion is changed from retrograde rotation to the oscillation is given by

$$r_{\rm p} < r_{\rm p,2} = \left(\frac{3}{6 + 2\sqrt{3}} \right)^{1/3} = 0.682. \tag{26}$$

Since the value of $r_{\rm p} = 0.8$ of Fig. 2 is between these two limiting values, the sliding phase can be maintained during retrograde rotation, but not after the sign of $\dot{\theta}$ becomes positive, leading to an escape. It should be noted that Eqs. (25) and (26) are the conditions for the particle not to separate from the moonlet, whereas separation does not always result in escape. In practice we find that in order to actually escape from the moonlet after retrograde evolution, the value of $r_{\rm p}$ must be larger than about 0.76 (this is almost independent of the strength of friction), which is slightly larger than $r_{\rm p,2}$.

In Appendix A, we explain the effect of the friction on the sliding phase in detail, including analytical estimates for the energy dissipation.

3.2 Contribution of Sliding Orbits to Averaged Torque

[Figure 3]

Next we study what fraction of particles in the parameter space experience the sliding phase, and how they affect the equilibrium spin rate of the moonlet. Figures 3a and 3b show the final values of the spin change $\Delta\omega_{\rm p}$ and the Jacobi integral E, as functions of b, respectively, obtained by using the instantaneous impact model. Adopted parameters are the same as those in Fig. 2. It can be easily recognized that the final spin changes are much larger than those obtained due to first impacts for $b = 1.85$–2.0 and for $b = 2.2$–2.45. These orbits experience a cascade of consecutive impacts, that is, the sliding phase, and finally escape from the moonlet. The occurrence of the sliding phase is also confirmed by the final value of E which is smaller than

that corresponding to $C = 0$. From these results, it is expected that the equilibrium spin rate $\omega_{\rm p,eq}$ is much larger than that obtained by considering only the first impacts, because of the sliding orbits.

As we showed in Fig. 2, u_θ becomes very small during the sliding phase unless the strength of friction is too small. Thus, the spin in the sliding phase is approximately given by $\omega_{\rm p} - 1 \simeq \dot{\theta}$. From Eqs. (23) and (24), the condition for the particle to escape from the moonlet is found as $2\dot{\theta}^2 + 2\dot{\theta} - C > 3/r_{\rm p}^3$. Thus, the value of $\dot{\theta}$ at the time of escape, $\dot{\theta}_{\rm esc}$, is given by

$$\dot{\theta}_{\rm esc} \simeq \frac{-1 \pm \sqrt{1 + 2(C + 3/r_{\rm p}^3)}}{2}, \tag{27}$$

where the sign of $\dot{\theta}_{\rm esc}$ is always positive in the case of $e = i = 0$. The value of C at the time of escaping depends on the history until the escape. If the particle initially revolves around the moonlet in a retrograde direction, C decreases gradually, so that the value of C at the time of escaping is roughly 0. This leads to $\dot{\theta}_{\rm esc} = \Delta\omega_{\rm p} = 1.28$ for the parameters used in Fig. 3 ($r_{\rm p} = 0.8$ and $\omega_{\rm p,ini} = 1.0$). This value of $\Delta\omega_{\rm p}$ is roughly consistent, although slightly larger than that shown in Fig. 3. This overestimation is due to approximations $\omega_{\rm p} - 1 \simeq \dot{\theta}$ and $C = 0$. In fact, the latter approximation is bad especially for orbits with $b = 1.85 - 2.0$, since they loose much energy by large inelastic rebounds, and do not experience any retrograde revolution around the moonlet. It should be noticed that there also exist some captured orbits ($E < 0$) for $b \simeq 1.9$: for these orbits $\Delta\omega_{\rm p} = 0$.

4 EQUILIBRIUM SPIN RATE OF MOONLETS

Now we study the equilibrium spin rate of the moonlet. If the averaged spin change $\langle \Delta\omega_{\rm p} \rangle$ is positive, the torque exerted on the moonlet is also positive so that the spin rate of the moonlet increases and vice versa. With changing the initial spin rate $\omega_{\rm p,ini}$, we can obtain the equilibrium

spin rate $\omega_{\rm p,eq}$ for which the torque vanishes ($\langle \Delta\omega_{\rm p} \rangle = 0$). The collision rate $P_{\rm col}(e, i)$ of small particles per unit surface number density onto the moonlet is given by (e.g., Ida and Nakazawa 1989)

$$P_{\rm col}(e, i) = \int p_{\rm col}(e, i, b, \tau, \lambda) \frac{3}{2} b db \frac{d\tau d\lambda}{(2\pi)^2} \tag{28}$$

where $p_{\rm col} = 1$ for collision orbits and otherwise 0. Using this collision rate, the averaged final spin is given as

$$\langle \Delta\omega_{\rm p} \rangle (e, i, \omega_{\rm p,ini}) = \frac{1}{P_{\rm col}} \int \Delta\omega_{\rm p}(e, i, b, \tau, \lambda, \omega_{\rm p,ini}) p_{\rm col}(e, i, b, \tau, \lambda) \frac{3}{2} b db \frac{d\tau d\lambda}{(2\pi)^2}. \tag{29}$$

We assume that distributions of small particles with respect to b, τ, and λ are uniform.

[Figure 4]

Figure 4 shows an example of the averaged spin change $\langle \Delta\omega_{\rm p} \rangle$ as a function of the initial spin rate $\omega_{\rm p,ini}$. The instantaneous impact method was used, with the same parameters as used in Fig. 3: $e = i = 0$, $r_{\rm p} = 0.8$, $\varepsilon_{\rm t} = 0.9$, and $\varepsilon_{\rm n} = 0.5$. We obtain the equilibrium spin rate $\omega_{\rm p,eq} \approx 1.8$ at the zero point, by a linear interpolation using the nearest two points. In the same manner, we obtain the equilibrium spin rate also in other cases. In most of the cases, there is only one equilibrium solution. However, there are a few special cases which have two stable equilibrium solutions (see Appendix B).

As shown in Section 3.2 (see Fig. 3), the equilibrium spin rate is affected by the fraction of sliding and captured orbits relative to the total number of collision orbits. Therefore, to help to understand the dependence of the spin rate on various parameters, we define the capture and sliding probabilities. For the capture probability $C_{\rm cap}$ the definition introduced in Ohtsuki (1993) is used:

$$C_{\rm cap}(e, i, \omega_{\rm p,ini}) = \frac{1}{P_{\rm col}} \int p_{\rm cap}(e, i, b, \tau, \lambda, \omega_{\rm p,ini}) \frac{3}{2} b db \frac{d\tau d\lambda}{(2\pi)^2}, \tag{30}$$

where $p_{\rm cap}$ is 1 for collision orbits with final $E < 0$, and otherwise 0. In order to define the sliding probability in the same manner, we need an exact definition for sliding orbits. In the present paper, we treat orbits with $t_{\rm slid} > t_{\rm lim}$ and final $E > 0$ (thus excluding orbits that eventually are captured) as sliding orbits, where $t_{\rm slid}$ and $t_{\rm lim}$ are the total duration of the sliding phase and the limiting time, respectively. The sliding phase corresponds to $|\boldsymbol{c} \cdot \boldsymbol{v}| < v_{\rm crit}$ for the instantaneous model and to $\xi > 0$ for the force model. We adopt the limiting time as $t_{\rm lim} = \pi/(2\sqrt{3}) \sim 0.9$, which corresponds to the quarter of the period of infinitesimal oscillation around the subplanet points (see Eq. (38)). Using this definition of sliding orbits, the sliding probability $C_{\rm slid}$ is given by

$$C_{\rm slid}(e, i, \omega_{\rm p,ini}) = \frac{1}{P_{\rm col}} \int p_{\rm slid}(e, i, b, \tau, \lambda, \omega_{\rm p,ini}) \frac{3}{2} b db \frac{d\tau d\lambda}{(2\pi)^2}, \tag{31}$$

where $p_{\rm slid}$ is 1 for sliding orbits and otherwise 0.

Further, we define the averaged spin changes for sliding and non-sliding orbits, which are also helpful for understanding the following results. The averaged spin change of sliding orbits $\langle \Delta\omega_{\rm p} \rangle_{\rm slid}$ is defined as

$$\langle \Delta\omega_{\rm p} \rangle_{\rm slid}(e, i, \omega_{\rm p,ini}) = \frac{\int \Delta\omega_{\rm p}(e, i, b, \tau, \lambda, \omega_{\rm p,ini}) p_{\rm slid}(e, i, b, \tau, \lambda, \omega_{\rm p,ini}) \frac{3}{2} b db \frac{d\tau d\lambda}{(2\pi)^2}}{\int p_{\rm slid}(e, i, b, \tau, \lambda, \omega_{\rm p,ini}) \frac{3}{2} b db \frac{d\tau d\lambda}{(2\pi)^2}}. \tag{32}$$

Replacing $p_{\rm slid}$ by $p_{\rm non-slid}$, which is 0 for sliding (and also for captured) orbits and otherwise 1, the averaged spin change for non-sliding orbits $\langle \Delta\omega_{\rm p} \rangle_{\rm non-slid}$ can be obtained in the same manner.

4.1 Dependence of Spin Rate on $r_{\rm p}$

[Figure 5]

Figure. 5a shows the equilibrium spin rate $\omega_{\rm p,eq}$ as a function of $r_{\rm p}$ for the case $\varepsilon_{\rm n} = 0.5$ and $e = i = 0$. We compare the results for four different cases: for two different impact methods with two different strengths of friction ($\varepsilon_{\rm t} = 0.5$ and 0.9 for the instantaneous impact method, and $\ell_{\rm f} = 0.1$ and 0.4 for the force method, respectively). To aid understanding of this figure, we also show the equilibrium spin rate obtained by considering only the first impact of each particle with the moonlet, as would be appropriate in the case of instantaneous sticking. In addition, Fig. 6 shows the sliding and capture probabilities. For the case of large enough $r_{\rm p}$ (~ 2.0), the colliding particles escape immediately after the first impact, so that the equilibrium spin rate is almost the same as that obtained by the first impacts only. Further more, this value is very close to the theoretical value 1/4 obtained for the zero random velocity case when neglecting the mutual gravity and thus also multiple impacts and the possible sliding phase and/or capture (Salo 1987a, Ohtsuki 2003a, b)

On the other hand, although the obtained equilibrium spin rate depends on the impact method and the strength of friction, the equilibrium spin for $r_{\rm p} \sim 1$ is much larger than that promoted by first impacts only. This follows because significant fraction of colliding particles experiences the sliding phase which enhances the torque, as we showed in Fig. 3. For $r_{\rm p} > 0.8$, the sliding probability increases with decreasing $r_{\rm p}$, and also, $\dot{\theta}_{\rm esc}$ and $\Delta\omega_{\rm p}$ of the sliding orbits increase (see Eq. (27)). Hence, the equilibrium rotation rate increases with decreasing $r_{\rm p}$. For $r_{\rm p} < 0.7$, most of the colliding orbits are captured, and there are no sliding orbits. It means that all of the colliding orbits which experience a sliding phase longer than $t_{\rm lim}$ are captured finally. Thus, the equilibrium spin rate is mainly determined by captured orbits and almost equals the synchronous rotation rate.

As compared with Ohtsuki (1993), our capture probabilities for the cases of $r_{\rm p} = 0.7$ and 0.75 are significantly larger. Since friction was not included in his numerical calculations,

the Jacobi energies of the sliding orbits remained constant during the sliding phase. Thus, some of the orbits were able to continue their sliding motions indefinitely with positive Jacobi energies, and therefore were not counted as captured orbits in his paper. Since we include friction, however, the Jacobi energies of these orbits can decrease during the sliding phase and become finally negative. Hence, our capture probabilities become larger than those in the case without friction. For the case of $r_{\rm p} \leq 0.6$, the capture probabilities in the present paper are well consistent with those in Ohtsuki (1993). This suggests that for small $r_{\rm p}$ Jacobi energies of the colliding particles become typically negative already before they start the sliding motion.

4.2 Dependence on the Collisional Method and Friction

[Figure 6]

An interesting feature seen in Fig. 5 was that whereas for the force model an increased strength of friction leads to larger $\omega_{\rm p}$, the opposite was true for the instantaneous impact model, giving $\omega_{\rm p,eq}(\varepsilon_{\rm t} = 0.9) > \omega_{\rm p,eq}(\varepsilon_{\rm t} = 0.5)$. This is further illustrated in Fig. 6, showing the equilibrium spin rate $\omega_{\rm p,eq}$ as a function of $1 - \varepsilon_{\rm t}$ (for the instantaneous impact model) and $\ell_{\rm f}$ (for the force model,) in the case of $e = i = 0$, $r_{\rm p} = 1.0$, and $\varepsilon_{\rm n} = 0.5$. One of the most important characteristics of this figure is that $\omega_{\rm p,eq}$ obtained by the instantaneous model is generally larger than that by the force model. Also, $\omega_{\rm p,eq}$ seems indeed to have a peak around $1 - \varepsilon_{\rm t} = 0.1$ for the instantaneous impact model whereas $\omega_{\rm p,eq}$ increases monotonically with $\ell_{\rm f}$ for the force model.

[Figure 7]

In order to understand the difference between the impact methods, we examine the dependences of the characteristics of sliding and non–sliding orbits on the impact method and the strength of the friction. Figure 7a and 7b show $\langle \Delta\omega_{\rm p} \rangle_{\rm slid}$ and $\langle \Delta\omega_{\rm p} \rangle_{\rm non-slid}$ as functions of $1 - \varepsilon_{\rm t}$

and $\ell_{\rm f}$, for the parameter values of Fig. 6. We compare the results for two different values of $\omega_{\rm p,ini} = 0.5$ and 1.5, the equilibrium spin rate falling between these values. If we assume, like in Sec. 3.2, that $C = 0$ and $u_\theta = r_{\rm p}(\dot{\theta} - (\omega_{\rm p} - 1)) = 0$ (corresponds to strong friction) at the time of the escape after the sliding phase, then $\langle \Delta\omega_{\rm p} \rangle_{\rm slid}$ should be about 1.32 and 0.32 for $\omega_{\rm p,ini} = 0.5$ and 1.5, respectively. Indeed, when the strength of friction is increased, $\langle \Delta\omega_{\rm p} \rangle_{\rm slid}$ becomes close to these estimated values. For the case of weaker friction, $\omega_{\rm p}$ is less enhanced at the time of escape, since the spin rate can not adjust quickly enough to keep $u_\theta \sim 0$, resulting in smaller $\langle \Delta\omega_{\rm p} \rangle_{\rm slid}$. Thus, if the spin evolution of moonlet were determined only by sliding orbits, the equilibrium spin rate $\omega_{\rm p,eq}$ would increase with increasing the strength of friction. On the other hand, $\langle \Delta\omega_{\rm p} \rangle_{\rm non-slid}$ becomes smaller with increasing friction for $\omega_{\rm p,ini} \simeq \omega_{\rm p,eq}$. Also in the case of force model, similar trends of $\langle \Delta\omega_{\rm p} \rangle_{\rm slid}$ and $\langle \Delta\omega_{\rm p} \rangle_{\rm non-slid}$ are seen.

Thus, the strength of friction for which the largest value of $\omega_{\rm p,eq}$ is obtained is determined by the balance between these two contributions. For the instantaneous impact model, $\omega_{\rm p,eq}$ attains maximum for $1 - \varepsilon_{\rm t} \simeq 0.1$, for which value the contribution to the torque from non-sliding particles is small whereas $\langle \Delta\omega_{\rm p} \rangle_{\rm slid}$ is large. For the force model, the increase of $\langle \Delta\omega_{\rm p} \rangle_{\rm slid}$ with $\ell_{\rm f}$ is stronger, and $\omega_{\rm p,eq}$ simply becomes larger with increasing friction, the contribution of non-sliding particles being less important.

It is also evident from Fig. 7 that the smaller value of $\omega_{\rm p,eq}$ for the force model in comparison to the instantaneous model is due to a typically smaller value of $\langle \Delta\omega_{\rm p} \rangle_{\rm slid}$. In the force model, the strength of friction is proportional to the mechanical pressure between the slightly overlapping small particle and moonlet. Hence, the effect of friction is diminished immediately before escaping, which induces a smaller value of $\omega_{\rm p}$ at the time of escape, and thus, leads to smaller $\omega_{\rm p,eq}$.

4.3 Dependence on $\varepsilon_{\rm n}$

[Figure 8]

Although the normal coefficient of restitution is an important parameter affecting the orbits of small particles, $\omega_{\rm p,eq}$ is insensitive to $\varepsilon_{\rm n}$, unless $\varepsilon_{\rm n}$ is close to unity, or unless the effect of friction is very strong. This can be seen in Fig. 8 where we plot $\omega_{\rm p,eq}$ as a function of $\varepsilon_{\rm n}$, comparing the same four different cases as in Fig. 5. We also show the sliding probability which is found to depend strongly on $\varepsilon_{\rm n}$. If the effect of friction is weak, $\omega_{\rm p,eq}$ is determined almost solely by sliding orbits even if their fraction is not so large. Since the value of $\langle \Delta\omega_{\rm p} \rangle_{\rm slid}$ does not change so much for different values of $\varepsilon_{\rm n}$, $\omega_{\rm p,eq}$ is insensitive to $\varepsilon_{\rm n}$. However, if friction is strong enough, the contribution from non-sliding orbits becomes important, so that $\omega_{\rm p,eq}$ decreases with decreasing sliding probability. If $\varepsilon_{\rm n}$ is close to unity, most particles escape after the first rebound, and there are only few sliding orbits. Therefore $\omega_{\rm p,eq}$ becomes small, being practically identical to that obtained by considering just the first impacts, shown in Fig. 5. However, the case of $\varepsilon_{\rm n}$ close to unity is of a limited interest, as in this case the expected velocity dispersion is so high that no formation aggregates is expected (Salo 1992, 1995).

In the present paper, we assume that $\varepsilon_{\rm n}$ is constant, although generally it is expected to depend on the impact velocity. Typical collision velocity of small particles onto the moonlet is likely to be at least of the order of $r_{\rm p}$. In dimensional form, this velocity corresponds to $\simeq 0.1$ cm s^{-1} for moonlets with 10m radii in Saturn's outer A ring. According to laboratory experiments of collisions between ice particles with frosted surfaces, the value of $\varepsilon_{\rm n}$ for this impact velocity is about 0.5 (Bridges *et al* 1984), whereas $\varepsilon_{\rm n}$ is about 0.8 for impacts with frost-free surfaces (Supulver *et al* 1995). For the latter case, one can find that the enhancement of spin rates by sliding orbits is less effective from Fig. 8. However, if we consider 100m-sized moonlets, thus impacts with $\simeq 1$ cm s^{-1}, $\varepsilon_{\rm n}$ is smaller than 0.5 regardless of the surface conditions. In this case,

the equilibrium spin rate is almost the same as for a fixed $\varepsilon_n \simeq 0.5$

4.4 Dependence on the Random Velocity

So far, we have discussed the results only for the case $e = i = 0$. However, if there are large aggregates in rings, the random velocity of small particles, $v_r = \sqrt{e^2 + i^2}$, is enhanced due to gravitational scatterings by these aggregates. The magnitude of the velocity may depend on the abundance of moonlets, as well as on the optical depth of the ring. If aggregates are common, v_r is expected to be of the order of the escape velocity of these aggregates, $v_{esc} = \sqrt{6/r_p}$. On the other hand, if there are only few moonlets and the optical depth is large, then the energy dissipation in the mutual collisions of small particles between the encounters with the moonlets is likely to reduce v_r to a much smaller value than v_{esc}. For the case of identical particles without aggregates, v_r is also expected to be near the escape velocity of the small particles, although the exact value depends on collisional parameters such as ε_n (Salo 1995, Ohtsuki 1999).

[Figure 9]

Figure 9 shows $\omega_{p,eq}$ as a function of e, for a fixed ratio $e/i = 2$, in the case of $r_p = 1.0$, $\varepsilon_t = 0.9$, and $\varepsilon_n = 0.5$. Note that $e = 2.19$ corresponds to $v_r = v_{esc}$ in this case. In the figure, $\omega_{p,eq}$ decreases monotonically with e. In order to understand this result, we also plot the sliding probability C_{slid} and the averaged spin change of sliding particles $\langle \Delta\omega_p \rangle_{slid}$ for the case $\omega_{p,ini} = 1.0$. As shown by Fig. 7a, the contribution to the torque from non-sliding orbits is found to be insignificant for the case $\varepsilon_t = 0.9$, so we focus on the properties of sliding orbits. The figure indicates that C_{slid} decreases with e, though it varies very little for $e < 1.5$. The decrease of C_{slid} may reduce the $\omega_{p,eq}$. However, a more important point is that $\langle \Delta\omega_p \rangle_{slid}$ decreases with e, suggesting that sliding particles can escape with a much smaller value of $\dot{\theta}$ than that in the

two-dimensional case (Eq. (27)). Thus, it is this three dimensional effect which significantly reduces the equilibrium spin rate. Nevertheless, we find that the spin rate is still enhanced by sliding orbits even for a large e.

[Figure 10]

Figure 10a shows $\omega_{\rm p,eq}$ as a function of $r_{\rm p}$ for the case of $v_{\rm r} = v_{\rm esc}$, $e/i = 2$, and $\varepsilon_{\rm n} = 0.5$. We compare the results for the same four different friction cases as studied in Fig. 5, which was for $v_{\rm r} = 0$. Further, in Fig. 10b, we plot $C_{\rm cap} + C_{\rm slid}$ and $C_{\rm slid}$ for the corresponding parameters of Fig. 10a. Compared with the case of $e = i = 0$, now $\omega_{\rm p,eq}$ is smaller for all $r_{\rm p}$, and also $C_{\rm cap} + C_{\rm slid}$ becomes smaller. For $r_{\rm p} \leq 0.7$, $\omega_{\rm p,eq}$ is almost unity because of the captured orbits, regardless of the friction strength. For larger $r_{\rm p}$, $\omega_{\rm p,eq}$ decreases with $r_{\rm p}$ and depends on the friction strength. For $0.7 < r_{\rm p} < 1.2$, the dependence of $\omega_{\rm p,eq}$ is similar to that in the case of $v_{\rm r} = 0$: ω is larger for the instantaneous impact model than for the force model. Also, as in Fig. 5, $\omega_{\rm p,eq}(\varepsilon_{\rm t} = 0.9) > \omega_{\rm p,eq}(\varepsilon_{\rm t} = 0.5)$, and $\omega_{\rm p,eq}(\ell_{\rm f} = 0.4) > \omega_{\rm p,eq}(\ell_{\rm f} = 0.1)$. Since the value of $r_{\rm p}$ in most parts of the Saturn's rings is considered to be within the above range, the spin rates of embedded moonlets might constrain the physical parameters, if these rates can be determined by observations. For $r_{\rm p} > 1.2$, $\omega_{\rm p,eq}$ is about the same as or slightly smaller than that obtained by considering first impacts only (we confirmed that if we use $\varepsilon_{\rm n} \simeq 1$, $\omega_{\rm p,eq}$ is more accurately consistent with that by first impacts).

5 DISCUSSION

5.1 Comparison with Ohtsuki (2003a, b)

Ohtsuki (2003a, b) also address the topic of this paper, and his and our studies are complementary to each other. Taking into account the Rayleigh distribution of orbital eccentricities

and inclinations of impact particles, he estimated not only the systematic component but also the random component of the moonlet spin, which arises from the collisions of individual large impactors, not considered in our paper. In Ohtsuki (2003a), he obtained analytic results for the non-gravitating limit, and in Ohtsuki (2003b), based on the numerical orbital integrations, he showed the results for a large range of velocity dispersions but mainly for $r_{\rm p} = 1$, and found a good agreement with the analytic results for the high-velocity limit.

In the case of $e = i = 0$, we confirmed that our equilibrium spin rate for $r_{\rm p} = 1$, $\varepsilon_{\rm n} = 0.5$, and $\varepsilon_{\rm t} = 0.9$, is consistent with his results ($\omega_{\rm p,eq} \simeq 1.4$), and that our equilibrium spin rate approaches to his analytic result ($\omega_{\rm p,eq} = 1/4$) with increasing $r_{\rm p}$ (note that the self-gravity becomes negligible for large $r_{\rm p}$: see Fig. 4). For the three dimensional case with $e/i = 2$, he used velocity dependent $\varepsilon_{\rm n}$ (Bridges *et al.* 1984), and the effective value of $\varepsilon_{\rm n}$ is larger than 0.5 with his assumed moonlet size (1m). Therefore, the direct comparison with our results is difficult. However, our equilibrium spin rate for large $r_{\rm p}$ is roughly consistent with his analytic result ($\omega_{\rm p,eq} = 0.3665$: see Fig. 11). He found that the equilibrium spin rate taking into account the Rayleigh distribution of e and i is roughly equal to the value obtained with a fixed e provided that the fixed $e \simeq \langle e^2 \rangle^{1/2}$. Thus, our results for the case of $e/i = 2$ obtained with neglecting the eccentricity distribution may give reasonable estimates even for the general case with a distribution of e and i.

He also found that the effect of the random component on $\omega_{\rm p,eq}$ can be significant if the velocity dispersion is as large as the escape velocity and the large impacts are common. In this case, slow rotation of the moonlet in both prograde and retrograde direction would be possible. These large collisions would also be destructive if the moonlets are rubble-pile aggregates as we will discuss below.

5.2 Stability of Moonlets

Here we discuss the stability of rotating moonlets with a zero internal strength (rubble pile aggregates). The acceleration toward the center of the aggregate at the subplanet points is given by (Harris 1996)

$$g = \frac{3}{r_{\rm p}^2} - r_{\rm p}\omega_{\rm p}^2 - 2r_{\rm p}, \tag{33}$$

where the first, second, and third term represent self gravity, centrifugal force, and tidal force, respectively. Note that dimensionless quantities defined in Sec. 2 are used: e.g. the spin rate is normalized by the Keplerian angular velocity. This equation also follows from Eq. (22), with $g = -\ddot{r}$, evaluated for $r = r_{\rm p}$ with $\dot{\theta} = \omega_{\rm p} - 1$. If g is positive, a spherical aggregate is stable, as all other locations in its surface feel a weaker disrupting effect than that in the subplanet points.

In local N-body simulations, performed for various distances and internal densities of particles, aggregate formation takes place for $r_{\rm p} < 0.6$–0.7 (Salo 1995, Karjalainen and Salo 2003 in preparation). Strictly speaking, this result corresponds just to the *onset* of aggregate formation: due to limitations mentioned in Introduction, the actual fate and stability of the aggregates has not been evaluated, as the simulations so far performed lack the effect of continued collisions and accretion of particles arriving from adjacent unperturbed ring regions. In principle, this subsequent evolution might endanger the stability of the aggregates, if for example their spins would be strongly excited. However, based on the results of the current study this seems not probable: for the typical case of $v_{\rm r} = v_{\rm esc}$, the equilibrium spin rate $\omega_{\rm p,eq}$ we found is smaller than the synchronous rotation rate for all $r_{\rm p}$'s (see Fig. 10), whereas according to Eq. (33), the rotational instability would require $\omega_{\rm p}$ greater than 1.96, 1.45, 1.0 for $r_{\rm p} = 0.8$, 0.9, 1.0, respectively (see Fig. 11)

On the other hand, for the case of $v_{\rm r} = 0$, $\omega_{\rm p,eq}$ may attain values larger than unity, especially for the instantaneous impact model with $\varepsilon_{\rm t} \sim 0.9$ (see Fig. 5). In this case also g may

become positive for some parameter values. Such a small velocity dispersion could in principle be achieved if the random velocities of small particles are sufficiently damped by their mutual collisions between encounters with moonlets. This special situation, that a few moonlets would form in a ring that is otherwise stable against aggregate formation, might happen if the density of moonlets (or maybe their cores) is significantly larger than that of the other particles. Nevertheless, even for $v_r = 0$, if r_p is smaller than about 0.8, the moonlets are always stable (see Fig. 11).

There are also other important effects which tend to break the aggregates. One is their elongated shape. Generally, aggregates forming in *N*-body simulations do not have a spherical shape but are elongated in the radial direction due to planetary tide (for example, see Fig. 17 of Salo, 1995). Then, the gravity term becomes about $1/f$ times smaller than that for the spherical case given by Eq. (33) (Harris 1996; see also Eq. (1)), assuming that the aggregate is a prolate body with a long/short axes ratio f. For example, using $f = 2$ (as suggested by Fig. 17 of Salo, 1995), the stability criterion for a synchronously rotating aggregate becomes $r_p < 0.79$, which is a much more stringent condition than $r_p < 1$ for a spherical aggregate (Fig. 11). Even in this case, typical aggregates with $r_p < 0.7$ should remain rotationally stable, unless ω_p is significantly larger than unity. Nevertheless, the spin rates for elongated moonlets have not been calculated in the present study, and the possibility remains that ω_p promoted by impacts and accretion could be significantly different from that for a spherical case. Another related factor not considered in the present study is the effect of surface irregularities: clearly, a rubble pile aggregate can hardly be expected to have a smooth surface. In the non-gravitating case, such irregularities, or deviations from a regular shape, might promote larger spin rates, as suggested by theoretical studies and simulations (Salo 1987a,b). On the other hand, if we include the mutual gravity, irregularities might prevent particles from sliding on the moonlet,

which will reduce the spin rate of the moonlet. Therefore, it is uncertain if these effect promote larger spin rates or not, and further studies are required.

Other important effect limiting the growth of aggregates may be the mutual collisions between large aggregates (Barbara and Esposito 2002). Since the value of $r_{\rm p}$ is larger for equal-sized particles, these collisions themselves are destructive, and also they can significantly accelerate the spin rates of the aggregates, which may lead to a rotational instability.

5.3 Comparison of Spin Rates with N-body Simulations

As formulated in Sec. 2.3, the equilibrium spin rate $\omega_{\rm p,eq}$ also corresponds to the z-component of the mean spin rate for a collisional ring system of identical particles.

The case in N-body simulations to which we can directly compare our three-body results are the systems with small optical depth and rather large $r_{\rm p}$-value, thus excluding cases where gravitational wakes or aggregates form. Toyama (2001) (and personal communication with K. Ohtsuki) conducted local N-body simulations for the case of $r_{\rm p} = 1.0$ and $\tau_{\rm d} = 0.005$, where $\tau_{\rm d}$ denotes the optical depth. He used the instantaneous impact method with $\varepsilon_{\rm n} = 0.5$, and examined the dependence of the mean spin $\langle \omega_z \rangle$ on $\varepsilon_{\rm t}$. In the equilibrium state, the values of $\langle \omega_z \rangle$ that he found were about 0.60 and 0.45 for $\varepsilon_{\rm t} = 0.9$ and 0.5, respectively. Our results in Fig. 10 for $v_{\rm r} = v_{\rm esc}$ and $r_{\rm p} = 1.0$ indicate that $\omega_{\rm p,eq} = 0.65$ and 0.58 for $\varepsilon_{\rm t} = 0.9$ and 0.5, respectively. Thus, our results are consistent with his, the small differences being due to the fact that the actual equilibrium random velocity is slightly larger than the mutual escape velocity ($\langle e^2 \rangle^{1/2} \simeq 2.5$ in Toyama (2001), in comparison to $e = 2.19$ for $v_{\rm r} = v_{\rm esc}$). The agreement was further confirmed by some additional N-body simulations performed with the instantaneous impact method used in Salo (1995). For the above parameters, but utilizing more particles ($N = 500$) and longer duration ($T_{\rm dur} = 1000 T_{\rm K}$) ($N = 255$ and $T_{\rm dur} = 200 T_{\rm K}$ in Toyama 2001),

these new simulations gave $\langle\omega_z\rangle = 0.56 \pm 0.03$ and 0.55 ± 0.05 for $\varepsilon_t = 0.9$ and 0.5, respectively. Using data obtained by three body calculations and assuming an isotropic Gaussian distribution of v_r (which is roughly consistent with a Rayleigh distribution of e and i), we also calculated the spin rates for the same values of the root mean square of v_r as given by these N-body calculations, yielding about 0.60 and 0.57, respectively. Thus, besides confirming the validity of Toyama (2001) results, this agreement also shows the mutual consistency of our N-body and three-body calculations, performed by entirely different codes and methods.

In Salo (1995) some simulations for the identical particle case included particle spins and friction. The main difference to Toyama (2001) is that these simulations were performed for a larger optical depth. The adopted distance $a = 10^8$m and internal density $\rho = 900$kg m^{-3}, correspond to $r_p = 1.22$ for an identical particle pair ($\mu = 1$ in Eq. (4)), and to $r_p = 0.77$ for $\mu = 0$. Using the instantaneous model with $\varepsilon_n = 0.5$ and $\varepsilon_t = 0.5$, it was found that $\langle\omega_z\rangle = 0.66 \pm 0.09$ for $\tau_d = 0.4$. For the case of such a high τ_d, gravitational wakes form and the total velocity dispersion of the system, measuring largely the relative movement of wakes, was much larger than the mutual escape velocity. However, in the wakes, the orbital elements of nearby particles are aligned and the relative velocity inside them remains significantly smaller, still corresponding to almost the mutual escape velocity of individual particles (Salo, 1995, Daisaka and Ida 1999). Thus, we compare the results of these N-body simulation with our present calculations for $v_r = v_{esc}$ (Fig. 10). Our results shows that $\langle\omega_z\rangle \simeq 0.4$ for $r_p = 1.2$, which is much lower than that obtained in Salo (1995). There are at least two possible explanations for this discrepancy. One is that distribution of direction and velocity of impacts is modified in wakes, whereas we assume a uniform distribution of orbital elements (τ, λ, and b; see Sec. 4). Other possibility is that wakes act like particle clumps, so that the effective value of r_p becomes smaller for collisions between the clumps and individual particles. Note that $\langle\omega_z\rangle$ increases with

decreasing $r_{\rm p}$. For example, if we assume that the wakes can be treated as clumps containing 100 individual particles, then using $\mu = 0.01$ and $D = 0.7$ in Eq. (4) would give $r_{\rm p} = 1.03$. According to Fig. 10, this would already indicate $\langle \omega_z \rangle \simeq 0.6$. However, a detailed analysis of collisions in wakes is required, in order to actually determine which explanation, if either of the above, is valid.

Richardson (1994) also conducted simulations with almost same conditions as in Salo (1992, 1995), adopting a distribution of particle sizes. He found that $\langle \omega_z \rangle$ is between about 0.2 and 0.4. This is a number-averaged value for all the particles, so that it actually represents the mean value for the smallest particles. On the other hand, $\langle \omega_z \rangle$ becomes larger for larger particles, and $\langle \omega_z \rangle$ of the largest particles was as large as that obtained in Salo (1995) (see Table 2 of Richardson 1994). This size dependence is in principle simple to explain by the $v_{\rm r}$ dependence of $\omega_{\rm p,eq}$: the equilibrium spin rate $\omega_{\rm p,eq}$ decreases with $v_{\rm r}$ (Fig. 9). Because of the partial energy equipartition, smaller particles have a larger random velocity dispersion than the larger ones. Moreover, difference of the normalized velocity $v_{\rm r}$ is even more pronounced. Therefore, $\langle \omega_z \rangle$ is expected to be larger for larger particles. Again, a more detailed analysis of N-body experiments is needed.

6 CONCLUSION

Conducting three body integrations including friction and spins, we have determined the equilibrium spin rate $\omega_{\rm p,eq}$ normalized by the orbital angular velocity. The equilibrium spin rate corresponds to the spin rate of the moonlet in a equilibrium state if the moonlet is much larger than other particles, and also corresponds to the mean spin rate in a ring system with identical particles.

We have found that $\omega_{\rm p,eq}$ is enhanced by sliding orbits as compared with the mean spin rate determined by considering first impacts only. For the case of zero random velocity, $\omega_{\rm p,eq}$

becomes larger than unity for $r_p \sim 1.0$ in some range of strength of friction. With increasing the relative random velocity, $\omega_{p,eq}$ decreases. If the relative random velocity is as large as the mutual escape velocity, $\omega_{p,eq}$ is lower than unity for $r_p \sim 1.0$, but its value is still larger than that obtained by first impacts. For $r_p < 0.7$, captures happen after some collisions, by which $\omega_{p,eq}$ becomes almost unity for all the cases of collisional parameters.

Based on the obtained data of the equilibrium spin rate, we have discussed stability of rubble pile aggregates. If the relative random velocity of incident particles is small enough, aggregates become rotationally unstable for $0.8 < r_p < 1.0$ in some limited cases of the strength of friction. However, it might be rather special situations and aggregates are stable for larger random velocity. There might be other mechanisms which break aggregates such as collisions between large aggregates.

Compared with the mean spin velocities obtained by N-body simulations including spins, we have found a good agreement with our results if the optical depth adopted in N-body simulations is small enough. On the other hand, for the large optical depth case, in which gravitational wakes form, the simulated mean spin velocity is much larger than that predicted by our results. There are some plausible explanations for this discrepancy, but further studies are required to clarify which one is correct.

The next paper in this series will extend our studies to larger optical depths with various size distributions of ring particles, using local N-body simulations. Especially, the dispersion of spin rate, which has not been examined in the present paper, will be very important, for the interpretation of the infrared observation data that will be obtained in the Cassini mission (e.g., Spilker *et al.* 2002).

ACKNOWLEDGMENTS

This work is supported by the Academy of Finland and the Oulu University special research-unit grant. We are grateful to K. Ohtsuki, R. Karjalainen, and anonymous two referees for providing useful comments.

Appendix A: Effect of Friction on Sliding Motion

[Figure 12]

If the particle initially slides in a retrograde direction around the moonlet, the time scale of remaining on the moonlet for the particle is determined by the dissipation rate of C (thus E) in the case of $r_{\rm p,2} < r_{\rm p} < r_{\rm p,1}$. Figure 12 shows the dependence of the duration of the sliding phase on the strength of friction, $1-\varepsilon_{\rm t}$ and $\ell_{\rm f}$, for the two different impact methods, with parameter values fixed to those in Fig. 2. This figure shows that the duration of the sliding phase has a minimum (corresponds to maximal energy dissipation rate) around $1-\varepsilon_{\rm t} \sim 0.01$ for the instantaneous impact model and around $\ell_{\rm f} \sim 0.1$ for the force model. On the other hand, the duration of sliding becomes longer for both stronger and weaker friction. Small energy dissipation in the case of weak friction is quite natural. On the other hand, how can we understand the small energy dissipation for the case of strong friction? Apparently, if friction is strong enough, the spin velocity quickly adjusts so that the tangential component of relative velocity remains small during the sliding phase, resulting in small energy dissipation.

It is possible to estimate analytically the value of $\varepsilon_{\rm t}$ leading to strongest energy dissipation. Including friction and spins, the equations of motion in the sliding phase are, from Eqs. (11) and (12), and Eqs. (14) and (16), given by

$$\frac{d^2\theta}{dt^2} = -\beta\left(\dot{\theta}-(\omega_{\rm p}-1)\right)-\frac{3}{2}\sin 2\theta, \tag{34}$$

$$\frac{d\omega_{\rm p}}{dt} = \frac{5}{2}\beta\left(\dot{\theta} - (\omega_{\rm p} - 1)\right). \tag{35}$$

Here, β represents the strength of interaction between the small particle and the moonlet, defined by

$$\beta = \begin{cases} \frac{2}{7}\nu(1-\varepsilon_{\rm t}) & \text{(Instantaneous impacts)}, \\ -\frac{2}{7}\frac{\ddot{\xi}\ell_{\rm f}}{|\dot{\theta} - (\omega_{\rm p} - 1)|} & \text{(Force model)}, \end{cases} \tag{36}$$

where $\nu = g/(2u_{\rm n,crit})$ represents the collision frequency in the instantaneous impact model, with $g = 3/r_{\rm p}^2 - r_{\rm p}\dot{\theta}^2 - 2r_{\rm p}\dot{\theta} - 3r_{\rm p}\cos^2\theta$, which is of order of unity in the retrograde revolution if $r_{\rm p} \simeq 0.8$. Assuming that β is constant and using Eqs. (23) and (34), we obtain the equation describing energy dissipation as

$$\frac{dC}{dt} = \frac{2}{r_{\rm p}^2}\frac{dE}{dt} = -2\beta\dot{\theta}\left(\dot{\theta} - (\omega_{\rm p} - 1)\right). \tag{37}$$

It is rather complicated to derive the general solutions for θ and $\omega_{\rm p}$, but if we consider infinitesimal oscillation ($|\theta| \ll 1$) around $\theta = 0$, an approximative solution can be easily obtained. Though this is not the exact solution describing evolution around the moonlet, it helps to understand the dependency of energy dissipation on β. As we showed in Fig. 2, the basic motion of the particle is dominated by the potential, even if there is friction, suggesting that friction can be treated as a small perturbation. In the case the infinitesimal oscillation, the basic motion is given by

$$\dot{\theta} = c_1 \cos\sqrt{3}t, \tag{38}$$

where we have chosen the initial phase angle to be zero and c_1 is the amplitude of the oscillation. Substituting this solution into Eq. (35), we obtain

$$\omega_{\rm p} - 1 = c_1\frac{2.5\beta}{2.5^2\beta^2 + 3}\left(2.5\beta\cos\sqrt{3}t + \sqrt{3}\sin\sqrt{3}t\right) + c_2 e^{-2.5\beta t}, \tag{39}$$

where c_2 is an integration constant determined by the initial conditions. In the above, the exponential term becomes small after a certain time, so we neglect this term. Substituting Eqs. (38)

and (39) into Eq. (37), and averaging over one oscillation period, we obtain

$$\int_0^{2\pi/\sqrt{3}} \frac{dC}{dt} dt = -c_1^2 \frac{2\pi}{\sqrt{3}} \frac{3\beta}{2.5^2\beta^2 + 3}. \tag{40}$$

This has the maximum absolute value when $\beta = \sqrt{3}/2.5$.

Using this value let us calculate the most effective value of ε_t. In the case of infinitesimal oscillation around $\theta = 0$, $g = 3/r_p^2 - 3r_p$, equal to 2.3 for $r_p = 0.8$. Since we use $u_{n,crit} = 0.01$ in the instantaneous impact model, the collision frequency $\nu = g/(2u_{n,crit}) = 115$. In this case, the most effective energy dissipation is obtained for $1 - \varepsilon_t = 0.02$. This estimate is consistent with the results in Fig. 12, although a bit larger than obtained in orbital integrations. Experiments with other values of $u_{n,crit}$ also confirm the validity of the above approximative treatment.

Unfortunately, it is impossible to derive an analytic solution of the most effective value of ℓ_f for the force model, because β can not be treated as a constant. But as suggested by Fig. 12, the dependence of energy dissipation on the strength of friction is qualitatively similar to that for the instantaneous impact model. One interesting feature is that the duration of the sliding phase increases drastically around $\ell_f \sim 0.25$.

Appendix B: Multiple solutions for $\omega_{p,eq}$

[Figure 13]

Figure 13a shows a figure similar to Fig. 4 except for the case of $r_p = 1.2$ instead of 0.8. It is noticeable that there are two equilibrium slutions $\omega_{p,eq} = 0.43$ and 1.05 (see also Fig. 5). This phenomenon is caused by the change of orbital behavior around $\omega_{p,ini} = 1.0$. Figure 13b shows orbits of particles for two different values of $\omega_{p,ini} = 0.8$ and 1.2, respectively. The particle starts the sliding motion with the retrograde direction. If $\omega_{p,ini}$ is larger than about 1.0, the small particle can not go beyond the highest potential point $(x, y) = (0, 1.2)$, and it

changes its sliding direction to the prograde and escapes after that. On the other hand, for smaller value of $\omega_{\rm p,ini}$, the orbit continues sliding phase with the retrograde direction beyond the highest potential point and separates from the moonlet near the subplanet point, hitting the moonlet again before escaping. In the former case of orbits, the spin change $\Delta\omega_{\rm p}$ becomes large, due to the sliding phase in the prograde direction, whereas this does not happen for the latter case. Same phenomenon occurs also for other b's. Hence, the average value $\langle\Delta\omega_{\rm p}\rangle$ changes significantly around $\omega_{\rm p,ini} = 1.0$. Similar transitions of orbital behavior are found for other parameters if $r_{\rm p} \sim 1.2$. For example, if we use $\varepsilon_{\rm t} = 0.5$ and same other parameters as in Fig. 13b, transition of the orbit behavior happens around $\omega_{\rm p,ini} = 0.4$. However, this value is much smaller than $\omega_{\rm p,eq}$ so that this transition does not affect for obtaining $\omega_{\rm p,eq}$. Also for the case of force model, similar transitions are found, but the contribution to the torque from the sliding orbits themselves are not so significant for $r_{\rm p} = 1.2$. Anyway, this phenomenon happens only in very limited cases, and thus does not have a physical significance.

REFERENCES

Araki S. 1991. The dynamics of particle disks. III. Dense and spinning particle disks. *Icarus* **90**, 139–171.

Barbara J. M. and L. W. Esposito 2002. Moonlet collisions and the effects of tidally modified accretion in Saturn's F ring. *Icarus* **160**, 161–171.

Daisaka H. and S. Ida 1999. Spatial structure and coherent motion in dense planetary rings induced by self-gravitational instability. *Earth Planets Space* **51**, 1195–1213.

Daisaka H., H. Tanaka, and S. Ida 2001. Viscosity in a dense planetary ring with self-gravitating particles. *Icarus* **154**, 296–312.

Davidsson B. J. R. 1999. Tidal splitting and rotational breakup of solid spheres. *Icarus* **142**, 525–535.

Dilley, J. P. 1993. Energy loss in collisions of icy spheres: Loss mechanism and size-mass dependence. *Icarus* **105**, 225–234.

Dones, L. and S. Tremaine 1993. On the origin of planetary spins. *Icarus* **103**, 67–92.

French R. G. and P. D. Nicholson 2000. Saturn's rings II. Particle sizes inferred from stellar occultation data. *Icarus* **145**, 502–523.

Harris A. W. 1996. Effect of shape and spin on the tidal disruption of P/Shoemaker–Levy 9. *Earth Moon Planets* **72**, 113–117.

Hämeen–Anttila, K. A. and H. Salo 1993. Generalized theory of non–identical particles in a gravitational field. *Earth Moon Planets* **62**, 47–84.

Ida S. 1990. Stirring and dynamical friction rates of planetesimals in the solar gravitational field. *Icarus* **88**, 129-145.

Ida, S. and K. Nakazawa 1989. Collisional probability of planetesimals in the solar gravitational field. III. *Astron. Astrophys.* **224**, 303–315.

Ida, S. and K. Nakazawa 1990. Did rotation of the protoplanets originate from the successive collisions of planetesimals? *Icarus* **86**, 561–573.

Karjalainen, R. and Salo, H. 2001. Gravitational accretion of particles in Saturn's rings. *Bull. Am. Astron. Soc.*, **33**, 1061.

Leinhardt Z. M., D. C. Richardson, and T. Quinn 2000. Direct *N*-body simulations of rubble pile collisions. *Icarus* **146**, 133–151.

Lissauer J. and D. M. Kary 1991. The origin of systematic component of planetary rotation. I. Planet on circular orbit. *Icarus* **94**, 126–159.

Nakazawa K. and S. Ida 1988. Hill's approximation in the three–body problems. *Prog. Theor. Phys. suppl.* **96**, 167–174.

Ohtsuki, K. 1993. Capture probability of colliding planetesimals: Dynamical constraints on accretion of planets, satellites and ring particles. *Icarus* **106**, 228–246.

Ohtsuki, K. 1999. Evolution of particle velocity dispersion in a circumplanetary disk due to inelastic collisions and gravitational interactions. *Icarus* **137**, 152–177.

Ohtsuki, K. 2003a. Analytic calculation for the spin angular momentum of a moonlet due to inelastic collisions of ring particles. Submitted to *Celest. Mech. Dyn. Astron.*.

Ohtsuki, K. 2003b. On the rotation of a moonlet embedded in planetary rings. Submitted to *Icarus*.

Ohtsuki, K. and S. Ida 1998. Planetary rotation by accretion of planetesimals with nonuniform spatial distribution formed by the planet's gravitational perturbation. *Icarus* **131**, 393–420.

Petit J. –M. and M. Hénon 1986. Satellite encounters. *Icarus* **66**, 536–555.

Petit J. –M. and M. Hénon 1987. A numerical simulation of planetary rings. I. Binary encounters. *Astron. Astrophys.* **173**, 303–315.

Richardson D. C 1994. Tree code simulations of planetary rings. *Mon. Not. R. Astron. Soc.* **269**, 493–511.

Salo, H. 1987a. Collisional evolution of rotating, non–identical particles. *Earth Moon Planets* **38**, 149–181.

Salo, H. 1987b. Numerical simulations of collisions between rotating particles. *Icarus* **70**, 37–51.

Salo, H. 1992. Gravitational wakes in Saturn's rings. *Nature* **359**, 619–621.

Salo, H. 1995. Simulations of dense planetary rings. III. Self–gravitating identical particles. *Icarus* **117**, 287–312.

Salo, H., J. Schmidt, and F. Spahn 2001. Viscous overstability in Saturn's B-ring. I. Direct simulations and measurement of transport coefficients. *Icarus* **153**, 295–315.

Showalter M. R. 1991. Visual detection of 1981S13, Saturn's eighteenth satellite, and its role in the Encke gap. *Nature* **351**, 709–713.

Spahn F. and M. Sremčević 2000. Density patterns induced by small moonlets in Saturn's rings? *Astron. Astrophys.* **358**, 368–372.

Spilker L., C. Ferrari, M. Showalter, J. Cuzzi, R. Achterberg, J. Pearl, M. Flasar, V. Kunde, S. Edberg, B. Wallis, J Aiello, S. Edgington, Cassini CIRS Investigation Team 2002. Cassini CIRS observations of Saturn's rings. *Bull. Amer. Astron. Soc.* **34**, 900.

Sremčević M., F. Spahn, and W. J. Duschl 2002. Density structures in perturbed thin cold discs. *Mon. Not. R. Astron. Soc.* **337**, 1139–1152.

Supulver K. D., F. G. Bridges, and D. N. C. Lin 1995. The coefficient of restitution of ice particles in glancing collisions: Experimental results for unfrosted surfaces. *Icarus* **113**, 188–199.

Toyama D. 2001. Dynamical evolution of planetary ring particles including spins. Master thesis (in Japanease), Yamagata University.

Weidenschilling, S. J., C. R. Chapman, D. Davis, and R. Greenberg 1984. Ring particles: Collisional interactions and physical nature. In *Planetary Rings* (R. Greenberg and A. Brahic, Eds.), pp.367–415. Univ. of Arizona Press, Tucson.

Wisdom, J., and S. Tremaine 1988. Local simulations of planetary rings. *Astron. J.* **95**, 925–940.

Figure captions

Figure 1. Dependence of the r_p parameter on the semimajor axis a for Saturn's rings, with various values of the mass ratio μ, the volume filling factor of the moonlet D, and the internal density of particles ρ. The locations of main rings are also shown. If the aggregate is composed of identical particles, the typical volume filling factor found in N-body simulations is about 0.7, very close to the maximum packing limit of identical spheres, $\pi/(3\sqrt{2}) = 0.74$ (Salo 1995). In the case of size distribution, D can reach even 0.8.

Figure 2. (a) A typical example of a collision orbit including a sliding phase, shown in the rotating Hill frame, for the case of $e = i = 0$, $b = 2.3$, $r_p = 0.8$, and $\omega_{p,ini} = 1.0$. The method of instantaneous velocity change in impacts is used with $\varepsilon_n = 0.5$ and $\varepsilon_t = 0.9$. Note that the particle performs several tens of retrograde revolutions around the moonlet, as seen in the rotating frame, before the final escape. (b) Corresponding evolution of various quantities as a function of time (normalized by the orbital period $T_K(= 2\pi)$). In order from the top panel, the spin rate ω_p, the angular velocity of mutual revolution $\dot{\theta}$, the relative tangential velocity at the contact point including the spin velocity $u_\theta = r\dot{\theta} - r_p(\omega_p - 1)$, and the Jacobi integral E are shown, respectively.

Figure 3. Final values of the spin change $\Delta\omega_p$ (solid curve in the upper panel) and the Jacobi integral E (solid curve in the lower panel), as a function of b. The case with $e = i = 0$, $r_p = 0.8$, $\omega_{p,ini} = 1.0$, $\varepsilon_n = 0.5$, and $\varepsilon_t = 0.9$ is studied. A dashed curve in the upper panel represents the change of spin after the first impact: if it overlaps with the final value of the spin change, it means that this orbit leads to an escape immediately after the first rebound, whereas orbits which experience the sliding phase have much larger final spin changes than those obtained due to first impacts. A horizontal dot-dashed line in the lower panel represents the value of E

corresponding to $C = 0$. Note that the final values of C for orbits with the sliding phase are negative ($E < 0.75$ for $r_{\rm p} = 0.8$).

Figure 4. Averaged spin change $\langle \Delta\omega_{\rm p} \rangle$ (symbols) as a function of $\omega_{\rm p,ini}$, together with a corresponding linear fit, in the case of $e = i = 0$, $r_{\rm p} = 0.8$, $\varepsilon_{\rm n} = 0.5$, and $\varepsilon_{\rm t} = 0.9$. The equilibrium spin rate of the moonlet, for which $\langle \Delta\omega_{\rm p} \rangle = 0$, corresponds to 1.81.

Figure 5. (a) The equilibrium spin rate of the moonlet as a function of $r_{\rm p}$ in the case of $\varepsilon_{\rm n} = 0.5$. Four different cases are shown: two different impact methods with two different strength of friction: $\varepsilon_{\rm t} = 0.5$ and 0.9 for the instantaneous method, and $\ell_{\rm f} = 0.1$ and 0.4 for the force method, respectively. The equilibrium spin rate obtained by considering only the first impacts is also shown. The statistical errors estimated by simulations using different grids in the impact parameter b (but with the same Δb), are smaller than the size of each mark. For $r_{\rm p} \sim 1$, the equilibrium spin rate is enhanced by particles experiencing the sliding phase, while for $r_{\rm p} < 0.7$, $\omega_{\rm p} \sim 1$ due to the captured orbits. Two stable equilibrium solutions exist around $r_{\rm p} = 1.2$ for $\varepsilon_{\rm t} = 0.9$: the lower values are represented by the dashed curve. (b) Capture and sliding probabilities corresponding to parameters of (a), but only for $\varepsilon_{\rm t} = 0.9$ (these probabilities are almost independent of the impact method and the strength of friction). The dashed curve shows the capture probability obtained in Ohtsuki (1993) for the frictionless case with $\varepsilon_{\rm n} = 0.5$

Figure 6. Dependence of the equilibrium spin rate $\omega_{\rm p,eq}$ on the strength of the friction $1 - \varepsilon_{\rm t}$ and $\ell_{\rm f}$ for the two different impact methods. The used parameters are $r_{\rm p} = 1.0$ and $\varepsilon_{\rm n} = 0.5$.

Figure 7. (a) The averaged spin change for sliding ($\langle \Delta\omega_{\rm p} \rangle_{\rm slid}$: solid curves) and non–sliding orbits ($\langle \Delta\omega_{\rm p} \rangle_{\rm non-slid}$: dashed curves) as a function of $1 - \varepsilon_{\rm t}$, shown for two different values of

$\omega_{\rm p,ini} = 0.5$ and 1.5. Instantaneous impact method is used. Indicated values 1.32 and 0.32 are the theoretical maximum values of the averaged spin change for $\omega_{\rm p,ini} = 0.5$ and 1.5, respectively (see Eq. (27)). (b) Same as (a) but using the force method.

Figure 8. Dependence of $\omega_{\rm p,eq}$ on $\varepsilon_{\rm n}$ for the case of $e = i = 0$ and $r_{\rm p} = 1.0$. Four different cases are shown: $\varepsilon_{\rm t} = 0.5$ and 0.9 for the instantaneous method, and $\ell_{\rm f} = 0.1$ and 0.4 for the force method, respectively. The sliding probability for the case of $\varepsilon_{\rm t} = 0.9$ and $\omega_{\rm p,ini} = 1.0$ (dashed curve) is also shown (being almost similar for all four cases and for different $\omega_{\rm p,ini}$).

Figure 9. Dependence of $\omega_{\rm p,eq}$ on the reduced eccentricity e, with a fixed ratio $e/i = 2$. The instantaneous method is used with $\varepsilon_{\rm t} = 0.9$, $\varepsilon_{\rm n} = 0.5$ and $r_{\rm p} = 1.0$. The averaged spin velocity for sliding orbits and the sliding probability for the case of $\omega_{\rm p,ini} = 1.0$ are also shown, as well as the spin rate obtained if only first impacts are used. The equilibrium spin rate decreases with increasing e, since the enhancement by sliding orbits becomes less effective.

Figure 10. (a) Same as Fig. 5 but for the case of non-zero random velocity, $v_{\rm r} = v_{\rm esc}$, with $e/i = 2$. Error bars are shown only for $\varepsilon_{\rm t} = 0.9$ and $\ell_{\rm f} = 0.1$. The equilibrium spin rate is much smaller than that for $e = i = 0$, but is still enhanced by sliding orbits as compared with the spin rate obtained by first impacts, for $r_{\rm p} \sim 1$. (b) Capture and sliding probabilities corresponding to parameters of (a) with $\omega_{\rm p,ini} = 1.0$.

Figure 11. The minimum spin rate required for the rotational instability of a strengthless aggregate as a function of $r_{\rm p}$ parameter, for the case of $f = 1$ (dashed curve) and $f = 2$ (dotted curve). The equilibrium spin rates $\omega_{\rm p,eq}$ for the case of $v_{\rm r} = 0$ and $v_{\rm esc}$ (solid curves) obtained by using the instantaneous method with $\varepsilon_{\rm t} = 0.9$ are also shown. The smaller value of $v_{\rm r}$ and the

larger value of f make the moonlet more unstable.

Figure 12. Dependence of the duration of the sliding phase on the strength of friction, measured by $1 - \varepsilon_t$ in the instantaneous impact model, and by ℓ_f in the force model. Values of other parameters are the same as those in Fig. 2. The longer duration of the sliding phase corresponds to a smaller energy dissipation rate.

Figure 13. (a) Same as Fig. 4 but for the case of $r_p = 1.2$. Note that there are two stable equilibrium spin rates, $\omega_{p,eq} = 0.43$ and 1.05. (b) Examples of orbits with different values of $\omega_{p,ini} = 0.8$ and 1.2, in the case of $r_p = 1.2$, $e = i = 0$, $b = 2.4$, $\varepsilon_t = 0.9$, and $\varepsilon_n = 0.5$.

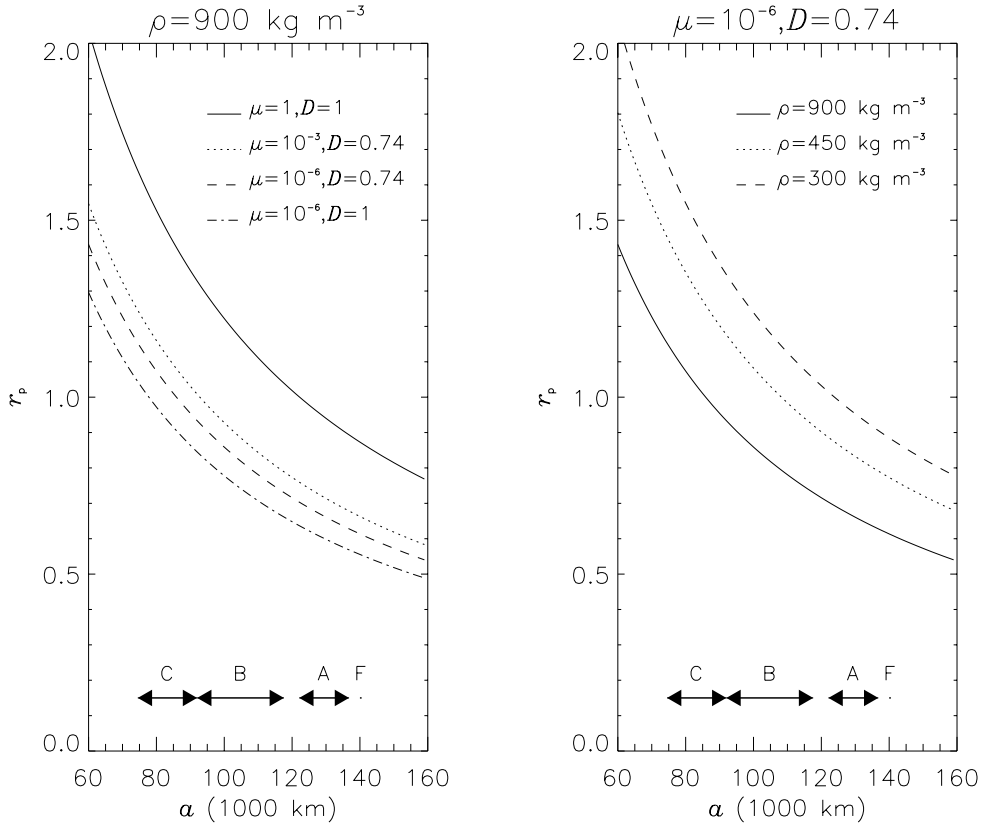

Figure 1. — Morishima and Salo, Spin rates of moonlets in rings

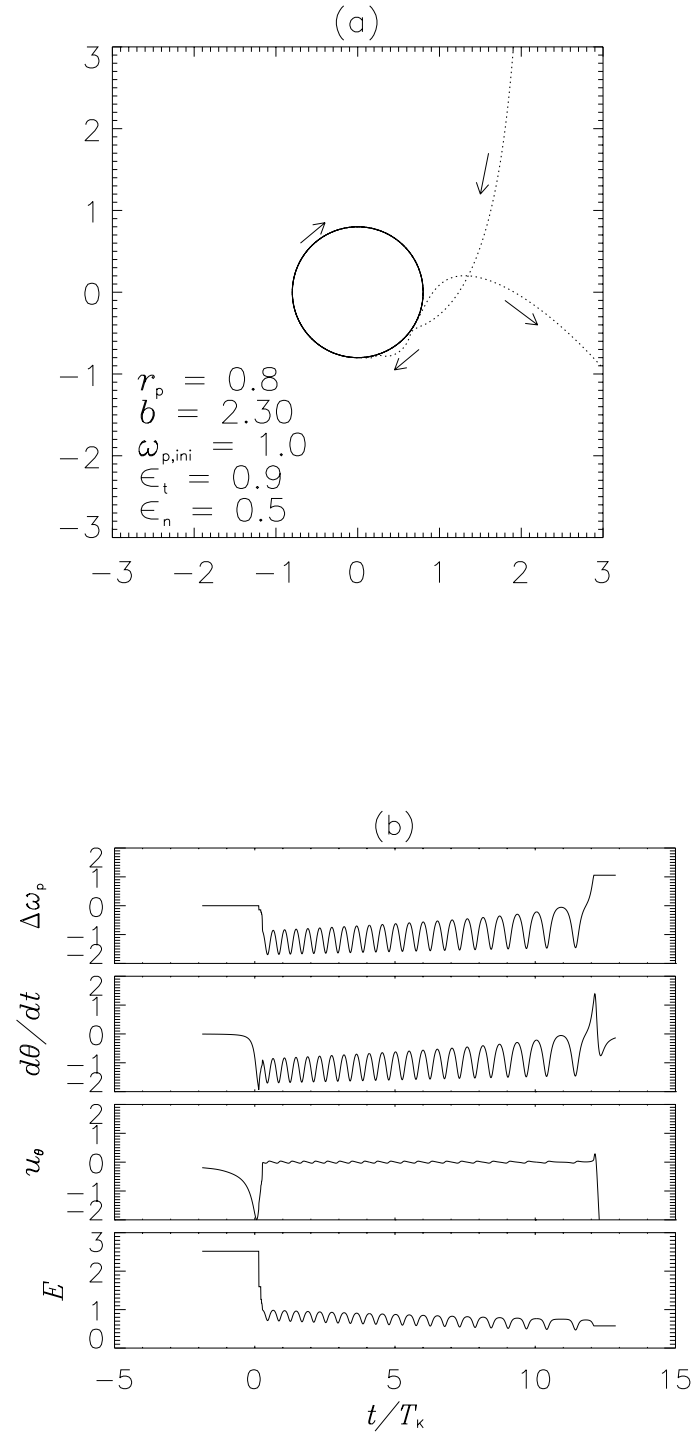

Figure 2. — Morishima and Salo, Spin rates of moonlets in rings

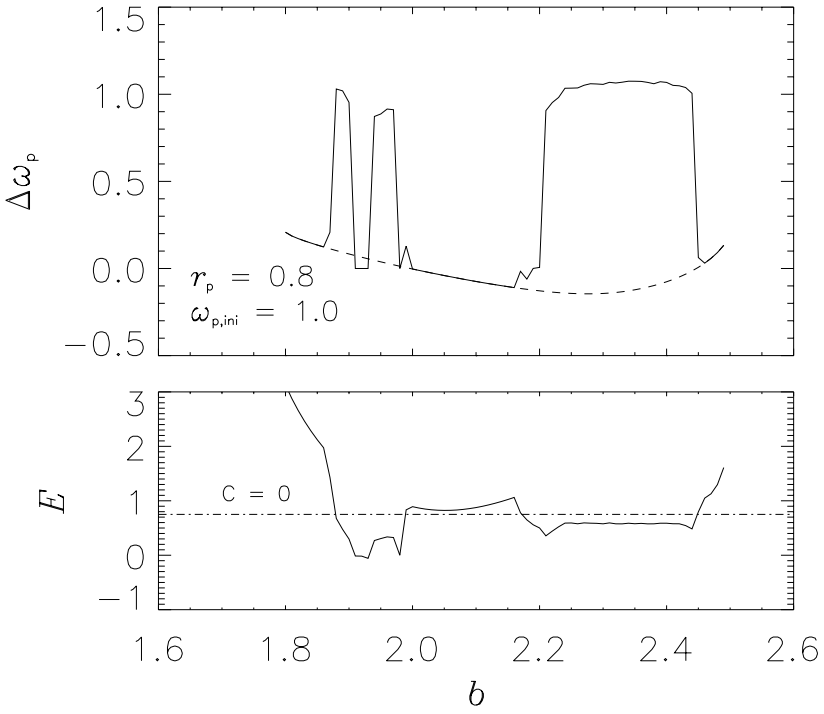

Figure 3. — Morishima and Salo, Spin rates of moonlets in rings

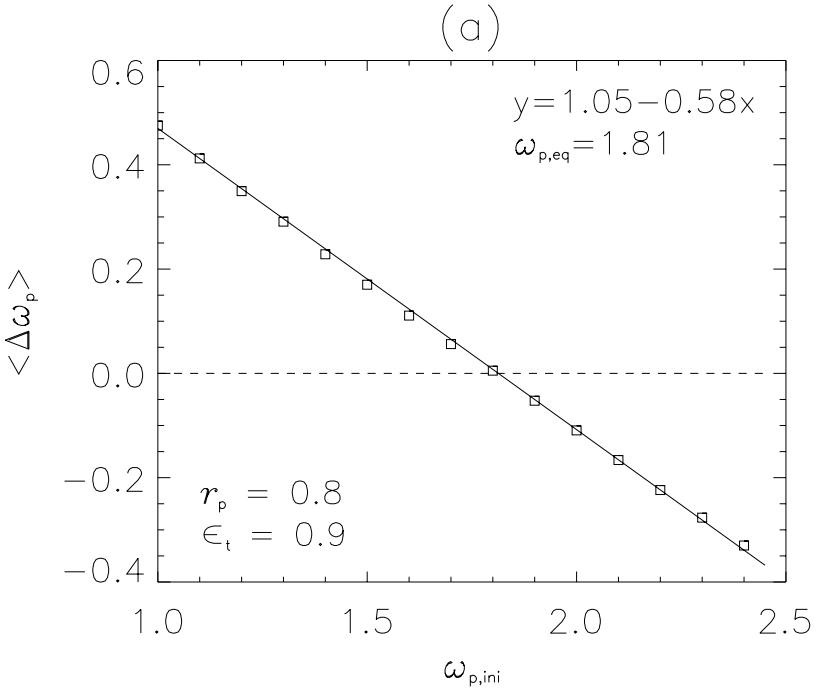

Figure 4. — Morishima and Salo, Spin rates of moonlets in rings

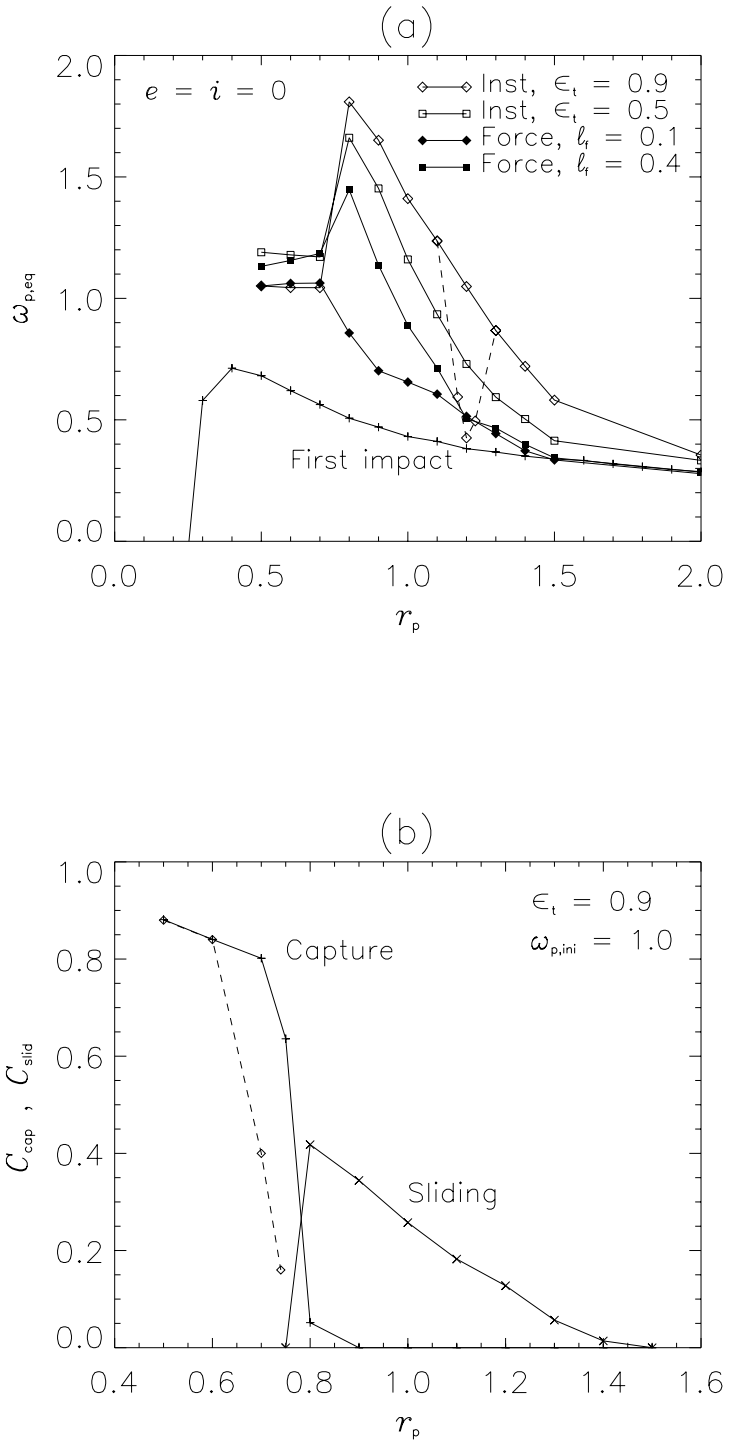

Figure 5. — Morishima and Salo, Spin rates of moonlets in rings

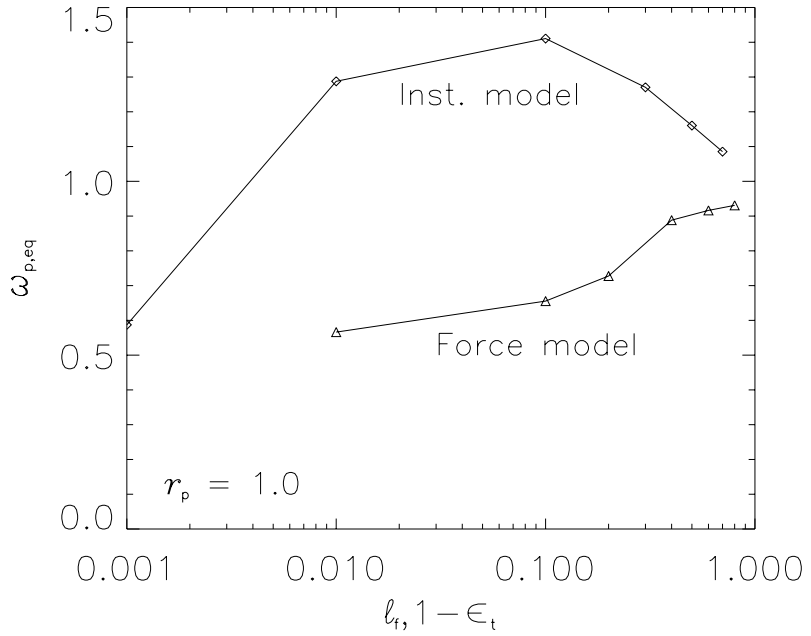

Figure 6. — Morishima and Salo, Spin rates of moonlets in rings

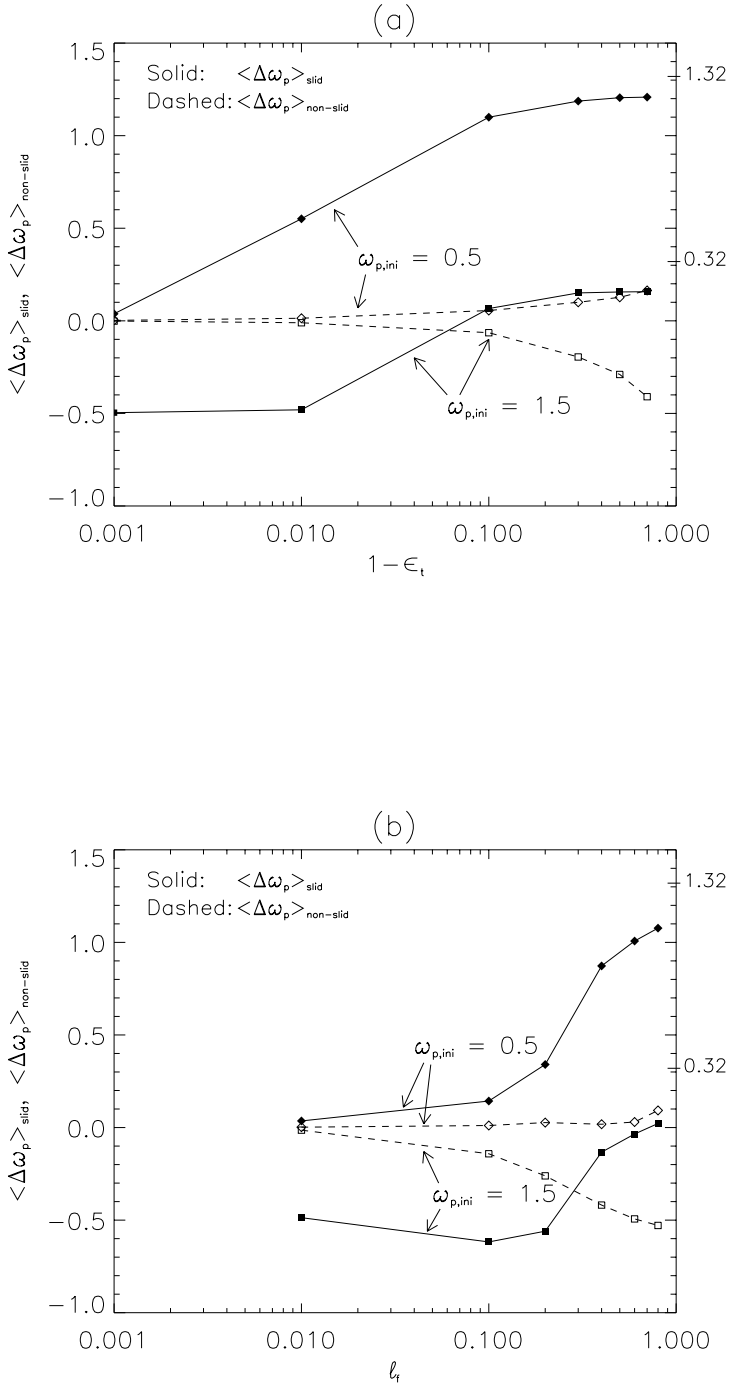

Figure 7. — Morishima and Salo, Spin rates of moonlets in rings

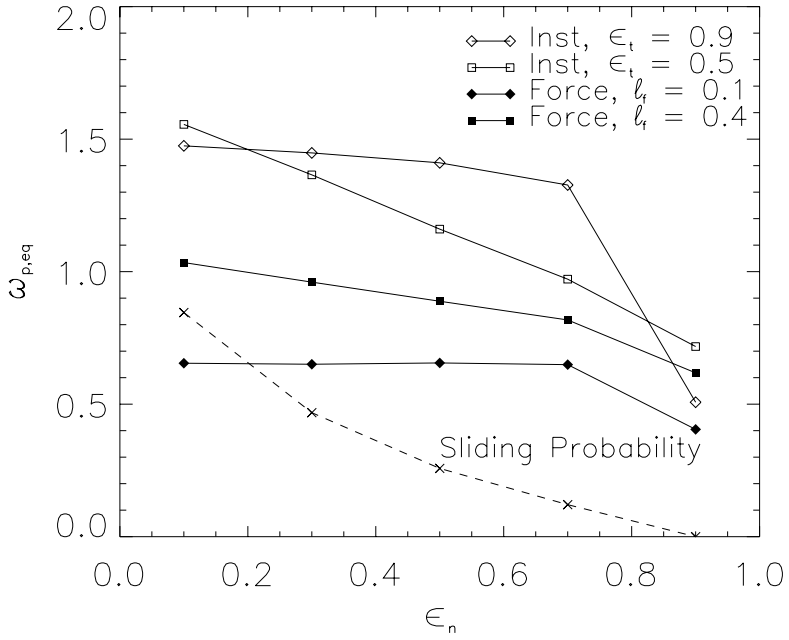

Figure 8. — Morishima and Salo, Spin rates of moonlets in rings

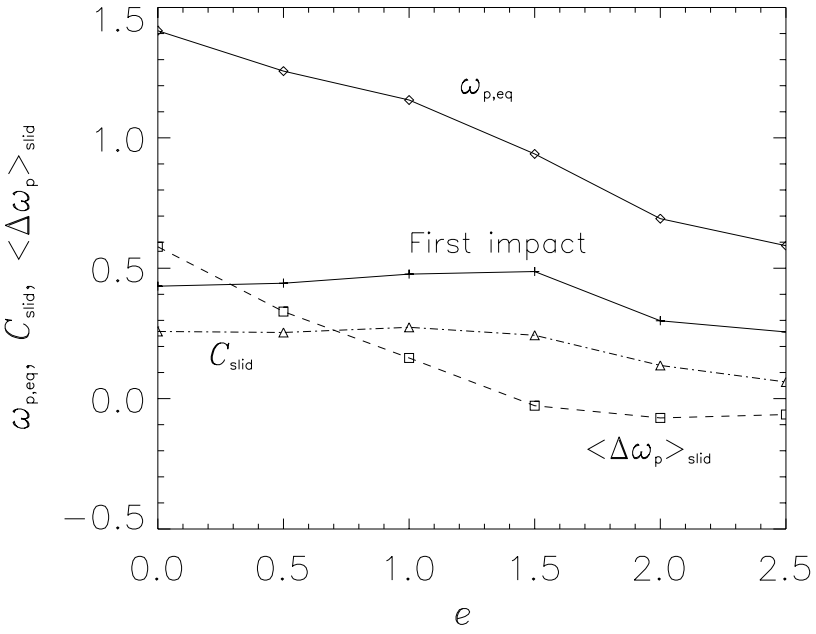

Figure 9. — Morishima and Salo, Spin rates of moonlets in rings

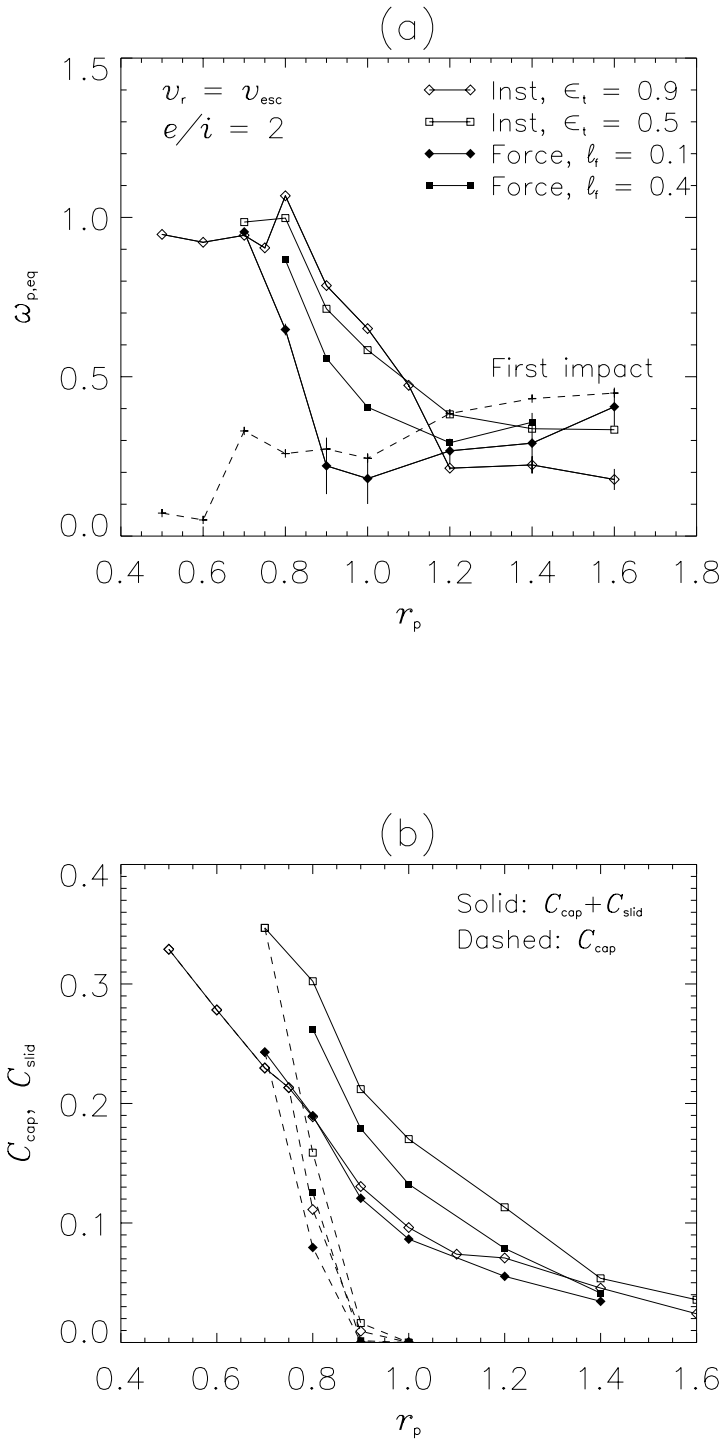

Figure 10. — Morishima and Salo, Spin rates of moonlets in rings

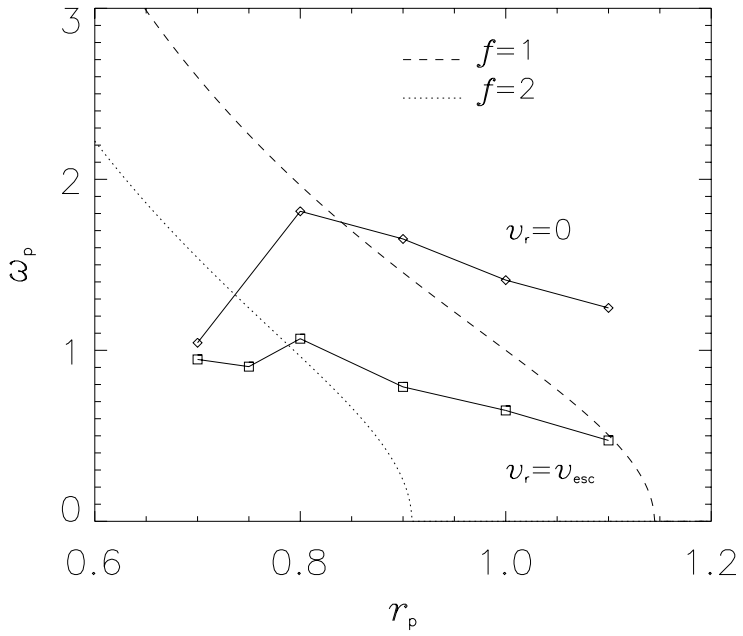

Figure 11. — Morishima and Salo, Spin rates of moonlets in rings

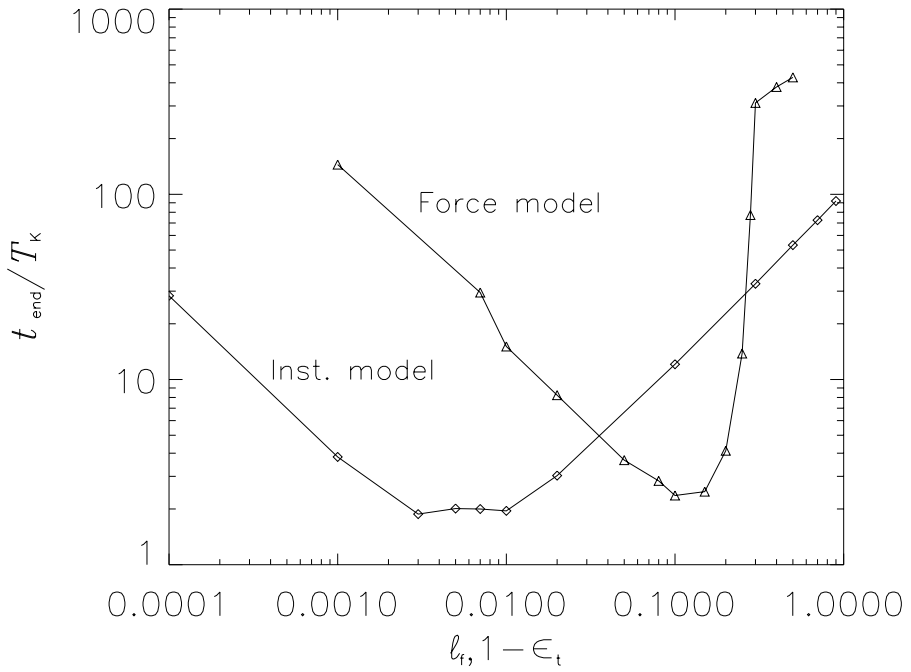

Figure 12. — Morishima and Salo, Spin rates of moonlets in rings

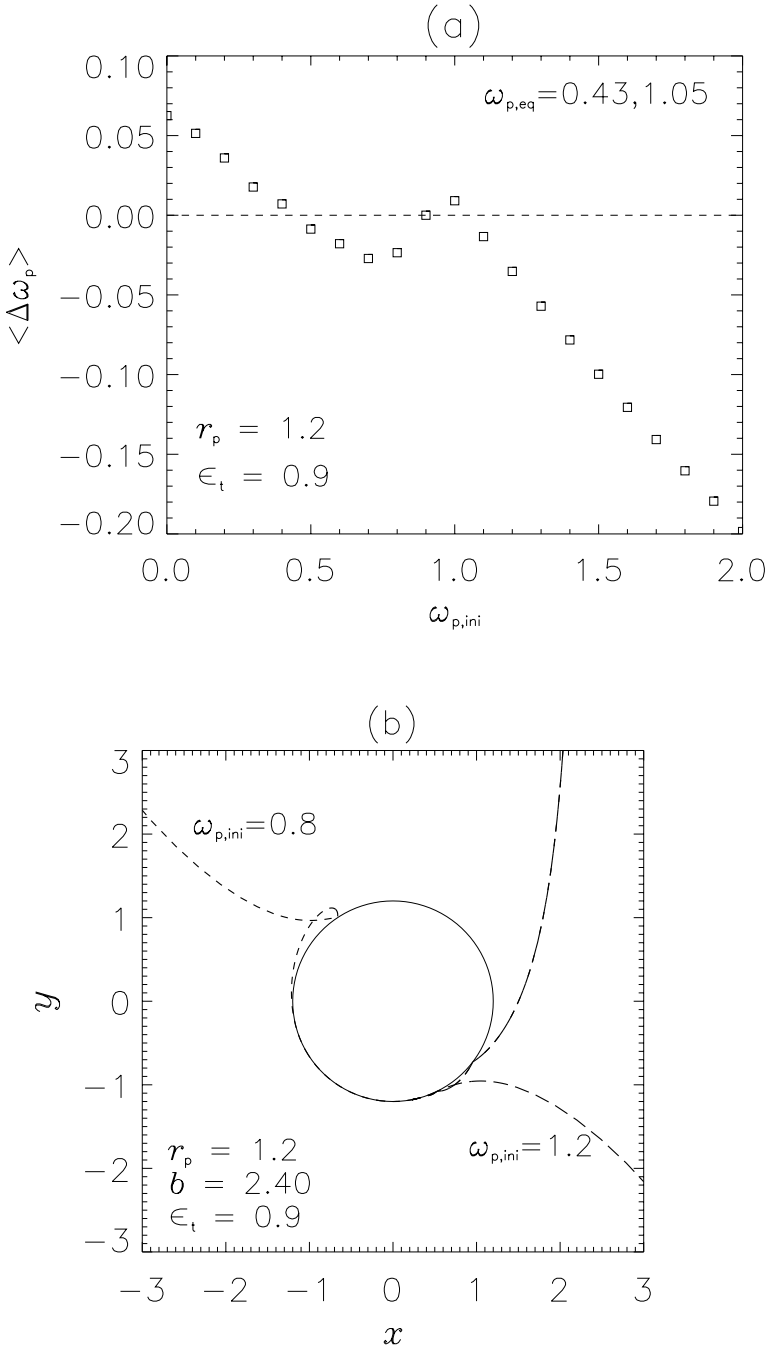

Figure 13. — Morishima and Salo, Spin rates of moonlets in rings